

An efficient stress recovery technique in adaptive finite element method using artificial neural network



A.R. Khoei^a, H. Moslemi^{b,*}, M.R. Seddighian^c

^a Center of Excellence in Structures and Earthquake Engineering, Department of Civil Engineering, Sharif University of Technology, P.O. Box 11365-9313, Tehran, Iran

^b Department of Civil Engineering, Shahed University, Tehran, Iran

^c School of Civil Engineering, Iran University of Science and Technology, Tehran, Iran

ARTICLE INFO

Keywords:

Stress recovery method
Artificial neural network
Adaptive FEM
Error estimation
Mesh refinement

ABSTRACT

In this paper, an efficient stress recovery technique is presented to estimate the recovered stress field at the nodal points. The feed-forward back-propagation multilayer perceptron (MLP) neural network approach is employed to improve the accuracy of the stress recovery method. An automatic adaptive mesh refinement is performed based on a-posteriori Zienkiewicz-Zhu error estimation method. The proposed technique is employed to recover the stress field accurately in the regions with a high stress gradient where the conventional recovery techniques are not able to improve the stress fields efficiently due to the singular behavior of problem. Finally, several numerical examples are solved to demonstrate the efficiency and accuracy of the proposed computational algorithm. The results are compared with the conventional methods, including the averaging method, superconvergent patch recovery (SPR) technique, and weighted superconvergent patch recovery (WSPR) method that illustrates how the artificial neural network can be used accurately to recover the stress field.

1. Introduction

The development of an efficient error estimation in numerical analysis of complex structures is one of the challenging problems in recent decades. The adaptive finite element method can be used as an efficient technique to create an optimal mesh with minimum degrees-of-freedom while producing an acceptable error. In this technique, the mesh is refined in such a way that the error can be distributed uniformly throughout the domain. Thus, the error estimation is a main part of the adaptive finite element method. Since the exact solution is not available in most practical problems, the error value must be estimated approximately. For this purpose, an improved solution is applied as an estimation of the exact solution. The recovery based technique introduced originally by **Zienkiewicz and Zhu** [1] proposes a recovery approach to obtain more accurate representation of the variables. The technique was introduced in the simplest form of averaging at each nodal point, and then was improved by employing the superconvergence concept to evaluate the recovered values more realistic. The concept of superconvergence expresses that the rate of convergence of the finite element solution at some points of the problem domain is higher than other points. **Zienkiewicz and Zhu** [2] presented that the gradients of the finite element solution are superconvergent at the Gauss integration points. They also highlighted that for some elements, such as triangular elements where the superconvergent points do not exist, certain sampling points still result in superconvergence of recovered values [3]. **Wiberg et al.** [4] improved the recovery of derivatives near the boundaries, where the tractions

* Corresponding author.

E-mail address: h.moslemi@shahed.ac.ir (H. Moslemi).

or displacements are prescribed by including the weighted residual errors at boundary points in the patch recovery. **Zhang and Zhu** [5] presented that the patch recovery technique yields to the superconvergence recovery for the gradient in both the L_2 -norm and L^∞ -norm, and the error estimator based on the recovered gradient is asymptotically exact.

The stress recovery and a-posteriori error estimation processes were employed by **Lee and Zhou** [6] within the element free Galerkin method (EFGM) using a general recovery approach called the weighed continuous moving-least-square recovery scheme. An improvement of the SPR technique, called the constrained SPR, was presented by **Ródenas et al.** [7] by applying the appropriate constraint equations in order to obtain the stress interpolation polynomials, which locally satisfy the equations that are satisfied by the exact solution. **Khoei et al.** [8] modified the SPR technique based on the recovery of gradients in crack problems using the analytical crack-tip fields in order to obtain more accurate estimation of errors. **Moslemi and Khoei** [9] developed the weighted superconvergent patch recovery (WSPR) technique particularly in crack problems that was significantly improved the stress fields at the boundaries as well as the elements located near the crack tip. **Payen and Bathe** [10] proposed a stress recovery procedure to improve the stress fields in the static, dynamic and nonlinear analysis of solids using the low-order displacement-based finite element method. **González-Estrada et al.** [11] presented an enhanced version of the SPR technique that was employed in a goal-oriented error estimator to provide a statically admissible stress field. The recovery technique was employed by **Kumar et al.** [12] to transfer the state variables between three-dimensional unstructured meshes by employing different variants of the recovery techniques based on the nodal patches and/or element patches. **Kumar et al.** [13] applied the SPR technique in an isogeometric analysis and derived the superconvergent points in the finite element solution based on the B-splines and LRB-splines in elliptical problems. **Sharma et al.** [14] proposed a stress recovery technique for low-order FEM, where the recovered stress field was obtained by satisfying equilibrium in an average sense. **Moslemi and Tavakkoli** [15] proposed an error estimation approach based on the statistical distribution of the stress values at each Gauss point to obtain the optimal FE mesh. **Kaveh and Seddighian** [16] presented a stress recovery technique using a metaheuristic algorithm called the Colliding Bodies Optimization to improve the stress field in fracture mechanics problems. **Lins et al.** [17] presented a stress recovery technique for the generalized/extended finite element method to compute the recovered stresses at re-entrant corners of any internal angle. An adaptive phase field method was proposed by **Jansari et al.** [18] for crack propagation in brittle materials based on the recovery type error indicator, which was combined with the quadtree decomposition.

The artificial neural network has been extensively used within the finite element methods to perform the structural analysis. **Takeuchi and Kosugi** [19] proposed the neural network representation of finite element method that consists of node-units and element-subnets whose synaptic weights are predetermined using the FEM. They updated the unknown inputs of the network to satisfy both the governing law and the boundary conditions. **Kowata et al.** [20] employed the Hopfield neural network to minimize the energy function obtained by the finite element analysis, and determined the selection of the sigmoid function and its influence on the iteration process. **Hurtado** [21] applied the radial basis function (RBF) within the neural network to evaluate the uncertainty in structural response prediction of one-dimensional stochastic finite elements. **Lefik and Schrefler** [22] proposed a back propagation artificial neural network as an incremental nonlinear constitutive model for the finite element analysis, in which the training process of the artificial neural network was accomplished by experimental data of a physically nonlinear body. **Hashash et al.** [23] applied a neural network based constitutive material model in finite element method, and derived a consistent material stiffness matrix that leads to efficient convergence of the FE Newton iterations. **Hambli et al.** [24] proposed an approach for virtual real-time deformation of complex structures by combining the neural network with FEM. **Ivirma et al.** [25] applied an artificial neural network for stress smoothing in hexaedrons that improves the stress fields of the finite element solution. **Park et al.** [26] presented a FE method by updating the boundary conditions using neural networks that was able to reduce the uncertainty of boundary conditions in FE model, and verified the accuracy of model through the laboratory tests and field tests on a steel girder bridge. **Stoffel et al.** [27] employed an artificial neural network in nonlinear structural mechanics by taking geometrical and material non-linearities into account. An application of the high-frequency acoustic emission system was proposed by **Ahn et al.** [28] based on the artificial intelligence for health monitoring of the pipeline to reduce the noise and redundant signal due to the high sensitivity transducer.

In the present paper, a stress recovery technique is presented based on the feed-forward back-propagation multilayer perceptron neural network in adaptive finite element method. The technique is developed to improve the accuracy of the recovered stress field at singular points. Since the conventional recovery techniques are not able to recover the stress fields at singular points accurately and several adaptive mesh refinement steps are required to attain the desired accuracy, an efficient stress recovery technique is presented here based on the neural network algorithm to accurately capture the singular stress fields. In the SPR technique, a polynomial field is generally fitted through the stress values of Gauss integration points, where the recovered nodal stresses are evaluated. This procedure may lead to misleading values of recovered singular stress fields and increase the computational costs of adaptive mesh refinements. However, it is shown here that the ANN technique is able to improve the recovered stress fields at singular points of complex problems. In this manner, the artificial neural network is trained to obtain the nodal stress values over each patch of elements. The training procedure is employed according to the values of Gauss integration points of each patch obtained from the finite element solution. It is highlighted that the efficiency of the proposed approach is obvious at stress singular points where the conventional recovery methods cannot capture the singularity accurately. This recovery strategy can be used in conjunction with an adaptive mesh refinement process to produce an appropriate mesh density. The plan of this article is as follows; **Section 2** briefly reviews the computation of fracture parameters in LEFM together with the crack initiation and crack growth direction. The error estimation and adaptive mesh refinement based on the SPR technique are represented in **Section 3**. **Section 4** introduces the proposed stress recovery technique based on the artificial neural network. In **Section 5**, several numerical examples are solved to illustrate the accuracy of the proposed computational algorithm over the conventional methods. Finally, several concluding remarks are given in **Section 6**.

2. Computation of fracture parameters in LEFM

In the linear elastic fracture mechanics (LEFM), the stress fields are introduced according to the stress intensity factors (SIF) at the crack-tip. So, it is significant to correctly calculate the SIFs in the finite element analysis of LEFM. There are a number of approaches presented in literature for calculation of the SIFs, including: the displacement correlation method, virtual crack extension method, modified crack closure integral, and J -integral method. Basically, the contour integral methods which are based on the energy release rate lead to more accurate SIFs. In this study, the stress intensity factors are computed from the FE solution on the basis of J -integral method. Since the evaluation of J -integral along a contour within the FEM mesh rarely demonstrates the path independence, the contour J -integral was transformed by Li et al. [29] to an equivalent area integral. Banks-Sills and Sherman [30] shown that the proposed equivalent area integral provides objective value for the J -integral with respect to the domain of integration. Consider a local coordinate system at the crack tip, where x_1 aligns with the crack axis and x_2 is perpendicular to the crack direction. The area J -integral can be defined as [31]

$$J = \int_A \left[\sigma_{ij} \frac{\partial u_i}{\partial x_1} - w \delta_{ij} \right] \frac{\partial q}{\partial x_j} dA \quad (1)$$

where w is the strain energy density defined as $w = \frac{1}{2} \sigma_{ij} \epsilon_{ij}$, δ is the Kronecker delta, q is a weighting function defined over the domain of integration, and A is the domain of integration around the crack tip, which encloses no other crack or void, as shown in Fig. 1. The weighting function q has a unit value on the inner contour C_1 , and zero value on the outer contour C_2 , as shown in Fig. 2. In the Gauss integration points of an element, q is interpolated over the element using the shape functions of an element as

$$q = \sum_{i=1}^{\text{Node}} N_i q_i \quad (2)$$

in which its derivatives in Eq. (1) can be obtained as

$$\frac{\partial q}{\partial x_j} = \sum_{i=1}^{\text{Node}} \frac{\partial N_i}{\partial x_j} q_i \quad (3)$$

It must be noted that if the inner contour C_1 shrinks onto the crack tip, Eq. (1) is still valid and converges to the value of J -integral. Although it was shown by Li et al. [29] and Blank-Sills and Sherman [30] that the domain of integration must be chosen far away

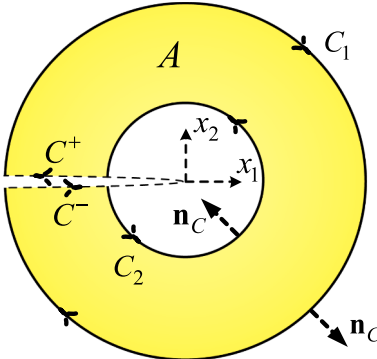


Fig. 1. The J -integral domain for computation of mixed mode stress intensity factors.

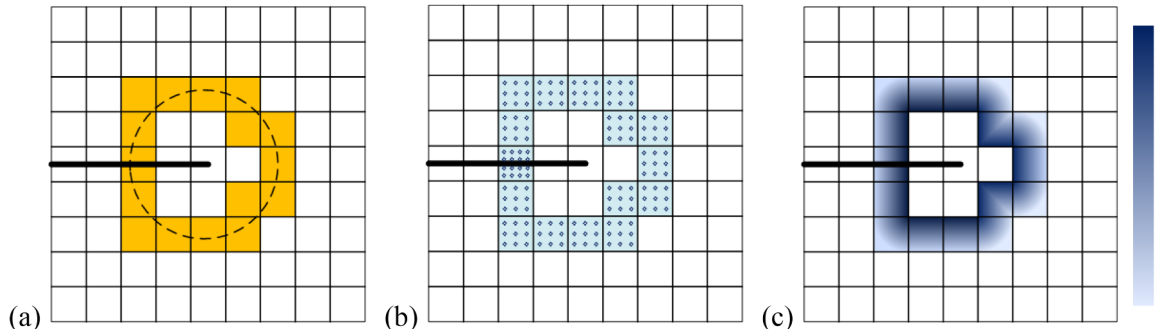


Fig. 2. Computation of the area J -integral; (a) Elements selected around the crack-tip, (b) Gauss integration points used for evaluation of the J -integral, (c) The distribution of weighting function q over the elements.

from the crack tip singularity, the incorporation of the artificial neural network in conjunction with the error estimation and adaptive mesh strategy improves the accuracy of the SIFs considerably at the crack tip region. As a result, the value of J -integral is obviously insensitive to the domain of integration [8], and the domain of integration can only be surrounded by the actual crack edges and it is not necessary to be selected far away from the crack tip.

In order to compute the values of fracture modes K_I and K_{II} from the area J -integral, the mode separation technique originally introduced by Ishikawa [32] and Bui [33] is applied here. In this method, the crack-tip displacement and stress fields are decomposed into the symmetric and anti-symmetric parts. The mode separated J -integral values J_I and J_{II} can then be obtained from Eq. (1) based on the decomposed displacement and stress fields. Hence, the stress intensity factors can be obtained by employing the mode separated J -integral values as

$$K_I = \sqrt{E' J_I} \quad \text{and} \quad K_{II} = \sqrt{E' J_{II}} \quad (4)$$

in which $E' = E$ for the plane stress and $E' = E/(1 - \nu^2)$ for the plane strain problems.

2.1. Crack initiation and crack growth direction

In practical problems, materials are generally subjected to mixed-mode loading conditions and computations of K_I and K_{II} are required. However, the fracture toughness of material is generally computed on the basis of pure mode I loading condition denoted by K_{IC} . Hence, a criterion must be defined to determine the fracture initiation that takes both stress intensity factors K_I and K_{II} into the account. Furthermore, the prediction of crack trajectory is significant in the analysis of material failure. So, a criterion is also required to determine the angle of crack growth with respect to the crack direction. There are different criteria proposed in literature; the most practical criteria are as follows, the maximum circumferential tensile stress criterion, maximum energy release rate criterion, and minimum strain energy density criterion.

The maximum circumferential tensile stress criterion that was originally proposed by Erdogan and Sih [34], is employed here to determine the crack initiation and crack growth direction. According to this criterion, the crack growth commences in a radial direction perpendicular to the direction of greatest tensile stress at the crack tip region. Furthermore, the crack initiation happens when the maximum circumferential tensile stress reaches its critical value. In fact, the circumferential tensile stress σ_θ reaches its maximum on a plane that the shear stress $\tau_{\theta\varphi}$ vanishes. Thus, the crack kinking angle can be defined as [35]

$$\theta_0 = 2\tan^{-1}\left(\frac{K_I}{4K_{II}} - \frac{1}{4}\sqrt{\left(\frac{K_I}{K_{II}}\right)^2 + 8}\right) \text{ for } K_{II} > 0 \quad (5)$$

$$\theta_0 = 2\tan^{-1}\left(\frac{K_I}{4K_{II}} + \frac{1}{4}\sqrt{\left(\frac{K_I}{K_{II}}\right)^2 + 8}\right) \text{ for } K_{II} < 0 \quad (6)$$

On the plane of crack propagation, the circumferential tensile stress is defined as

$$\sigma_{\theta-\max} = \frac{K_I}{\sqrt{2\pi r}} \cos \frac{\theta_0}{2} \left(1 - \sin^2 \frac{\theta_0}{2}\right) + \frac{K_{II}}{\sqrt{2\pi r}} \left(-\frac{3}{4} \sin \frac{\theta_0}{2} - \frac{3}{4} \sin \frac{3\theta_0}{2}\right) \quad (7)$$

The crack initiation occurs if $\sigma_{\theta-\max}$ reaches the critical value $K_{IC}/\sqrt{2\pi r}$. Thus, an equivalent stress intensity factor K_{eq} is defined for the mixed-mode conditions as

$$K_{eq} = K_I \cos^3 \frac{\theta_0}{2} - \frac{3}{2} K_{II} \cos \frac{\theta_0}{2} \sin \theta_0 \quad (8)$$

In all finite element simulations presented here, the stress intensity factors K_I and K_{II} are obtained from the area J -integral described above, which are more accurate. In this manner, the accurate values of stress fields can be obtained from the FE solution for implementation in the recovery process used through the artificial neural network. A detailed description of the crack initiation criterion employed to predict the angle of crack growth with respect to the crack direction can be found in [36–38].

3. Error estimation and adaptive remeshing

The error of spatial discretization is the principal source of error in the finite element method and various techniques have been proposed by researchers to reduce the discretization error. In adaptive finite element method, the optimal mesh is defined as a mesh with minimum DOFs, while the discretization error does not exceed the aim error. However, the exact solution is not available in most practical problems and the exact error cannot be computed. Hence, the exact solution is replaced by an improved solution to estimate the error. In the recovery techniques, the finite element solution is recovered to produce the improved solution properly. The recovery techniques range from a simple form of the averaging method with less accuracy to an accurate model of the superconvergent patch recovery (SPR) technique. It has been shown that the superconvergent points results in more accurate stress values than other points, and leads to the high rate of convergence. Moreover, the stress solutions are superconvergent at Gauss integration points [2]. In the SPR technique, a patch is defined for each vertex node including the Gauss points of elements, in which each

component of the stress is approximated by a polynomial of order p . Hence, the recovered solution can be obtained for each component of σ_i^* by

$$\sigma_i^* = \mathbf{P} \mathbf{a} = < 1 \ x \ y \ \dots \ y^p > < a_0 \ a_1 \ a_2 \ \dots \ a_n >^T \quad (9)$$

The unknown parameters of the polynomial a are determined by fitting the superconvergent values in a least square sense. Hence, the following error function must be minimized over the patch with a total sampling points m as

$$F(\mathbf{a}) = \sum_{k=1}^m (\sigma_i^*(x_k, y_k) - \hat{\sigma}_i(x_k, y_k))^2 = \sum_{k=1}^m (\mathbf{P}(x_k, y_k) \mathbf{a} - \hat{\sigma}_i(x_k, y_k))^2 \quad (10)$$

where (x_k, y_k) are the coordinates of the Gauss points in the patch and $\hat{\sigma}$ is the value of stress derived by a finite element solution. In the weighted SPR technique (WSPR), different weighting parameters are used for sampling points of the patch to obtain more realistic values of the recovered stress [9]. In this technique, the nearest sampling points have more effects in the recovery process. The corresponding weighting factor is taken as $w_k = 1/\eta_k$, where η_k denotes the distance of the k^{th} sampling point from the recovering node. Thus, the error function in Eq. (10) takes the following form in the WSPR technique as

$$F(\mathbf{a}) = \sum_{k=1}^m w_k (\mathbf{P}(x_k, y_k) \mathbf{a} - \hat{\sigma}_i(x_k, y_k))^2 \quad (11)$$

in which the vector a can be obtained by minimizing the error function $F(a)$ as

$$\mathbf{a} = \left(\sum_{k=1}^m w_k^2 \mathbf{P}_k^T \mathbf{P}_k \right)^{-1} \sum_{k=1}^m (w_k^2 \mathbf{P}_k^T \hat{\sigma}_i(x_k, y_k)) \quad (12)$$

The recovered stress field of the target nodal point can be obtained by evaluation of the fitting polynomial at the coordinates of that nodal point. The process of stress recovery is repeated for all nodal points of the domain and different polynomials are fitted over the patches. In Fig. 3, a representation of the stress recovery is illustrated schematically using the SPR technique. Since the sampling points are superconvergent, the approximation becomes superconvergent and the finite element solution is improved. The stress value at each Gauss point of the element can be obtained by employing the shape function on the nodal recovered stresses as

$$\sigma_G^* = \mathbf{N} \sigma_N^* \quad (13)$$

The discretization error is approximated as the difference between the improved solution and those given directly by the finite element solution as

$$e_\sigma \approx \sigma_G^* - \hat{\sigma} \quad (14)$$

where $\hat{\sigma}$ represents the stress value obtained from the FE solution and σ_G^* is the recovered stress. Basically, the distribution of error may be different over the domain; the regions with high values of stress gradient represent large values of error, while the regions with uniform stress distribution lead to the low value of error. According to the L_2 -norm of stress, the error of stress field can be normalized as

$$\eta = \frac{e_\sigma}{\|\hat{\sigma}\|} \quad (15)$$

In order to uniformly distribute the error throughout the domain, the aim error η_{aim} is defined that depends on the expected

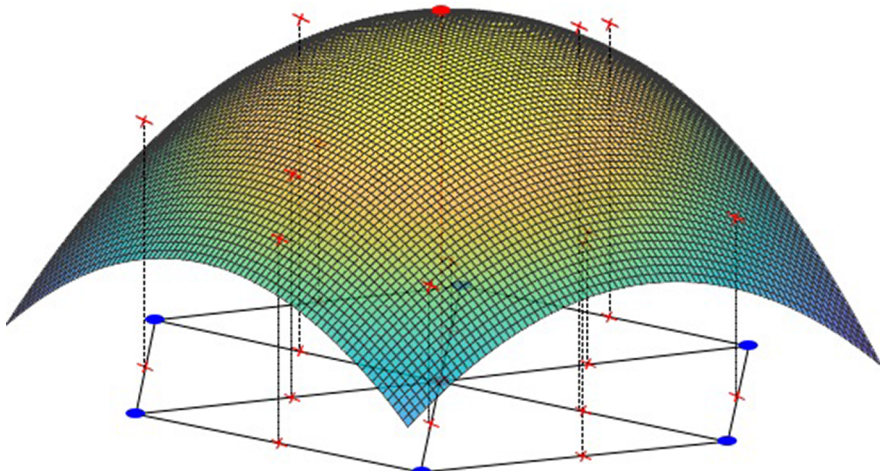


Fig. 3. The stress recovery using the SPR technique on a patch of elements.

accuracy of the solution. So, the mesh is generated by refining the elements with a high value of the error while coarsening the elements with a low value of the error. The rate of error convergence in isoparametric elements is proportional to the size of element. If $(h_i)_{old}$ denotes the i^{th} element size in the initial mesh, the new element size can be obtained as

$$(h_i)_{new} = \frac{\eta_{aim}}{\eta} (h_i)_{old} \quad (16)$$

The new element sizes form a mesh density that can be exported to a mesh generator to produce the new adaptive mesh. In order to avoid the mesh generation problems, the lower and upper limits are proposed for the element size. The pointwise estimated error may never reach the aim error in some critical points of the problem, such as the crack tip. Since the pointwise estimated error cannot evaluate the overall accuracy of the solution, a global error norm is defined as

$$\|e_\sigma\| = \left(\int_{\Omega} (\sigma_G^* - \hat{\sigma})^T (\sigma_G^* - \hat{\sigma}) d\Omega \right)^{1/2} \quad (17)$$

This global error is normalized with respect to the norm of stress and compared to the aim error. The multi-level adaptive mesh refinement may be required in some problems to attain the aim error. In such case, each refined mesh is taken as the initial mesh for the next level of adaptive remeshing. Since the estimated error and mesh refinement depend directly on the improved stress field, the stress recovery process is the most important part of this procedure.

4. Stress recovery using artificial neural network (ANN)

The stress recovery technique described in the preceding section suffers from an important drawback; in fact, the stress values of all nodal points of the domain are recovered by applying an identical procedure, while a uniform stress field may occur in some regions and the high gradient stress field happens in other regions. In such a case, the fitting procedure with a predefined polynomial function may cause inaccurate recovered stress fields over the domain. Hence, the recovery procedure must be improved considerably by applying a technique that is able to adapt itself to different regions. There are several techniques proposed in the literature to prevent such a drawback; for instance, the analytical solution of the asymptotic functions is incorporated in the SPR technique as the smoothing function at the crack-tip region [37]. The artificial neural network (ANN) is an alternative approach that can be used appropriately to recover the stress field in the adaptive mesh strategy. In what follows, the basics of the ANN architecture are first described, and the stress recovery technique is then implemented on the basis of the ANN technique.

4.1. The ANN architecture

The artificial neural network (ANN) is defined by the multiple layer configuration, in which the multilayer perceptron (MLP) neural network consists of simple components. In a single-point neuron, the simple neurons are stack together to produce the layers. The layers are then cascaded to build up the network. In a single-input neuron, the scalar input x , such as the coordinate of a node, is multiplied by the scalar weight coefficient w to build up wx ; a bias coefficient b is then added to produce the output n . The neuron input, which is called the summer output, incorporates into a transfer or activation function f to create the final scalar neuron output S , for example, the stress component of a node in a specific coordinate, as

$$S = f(wx + b) \quad (18)$$

The weight and bias coefficients are both adjustable scalar parameters. Generally, the transfer function is chosen by the operator, and the parameters w and b are adjusted by learning rules. Basically, the activation function takes the input into account and squashes the output into the range of $[0, 1]$. Since some initial data are available, for example, the stress components of a patch, it is possible to define the error as the difference between the available data and those predicted by neuron outputs. Hence, the weight and bias coefficients are modified until the error becomes less than a feasible value. Consider a neuron with R -inputs, such as the coordinates x , y and z , Eq. (18) can therefore be transformed to

$$S = f(w_1x_1 + w_2x_2 + w_3x_3 + \dots + w_Rx_R + b) \quad (19)$$

It is obvious that a single neuron, even with several inputs, is not sufficient to analyze a complicated function. In such case, several parallel operating, e.g. 5 or 10, are required that is called a layer. The layer includes the weight matrix w , the bias vector b , the activation function f , and the output vector S . The S -neurons, R -inputs, and one-layer network can be drawn in a matrix notation, as shown in Fig. 4. A network consists of several layers, in which each layer has its own weight matrix, a bias vector, a net input vector, and an output vector. The outputs of layers one and two are inputs for layers two and three. Such a similar manner forms the sequence of layers. A layer whose output is the network output is called an output layer, and the other layers are called the hidden layers. The error of the output neuron j at the n^{th} training sample can be defined as

$$e_j(n) = d_j(n) - y_j(n) \quad (20)$$

where $d_j(n)$ and $y_j(n)$ are the input value and predicted value of neuron j , respectively. It is possible to define the instantaneous value of the error energy for neuron j as

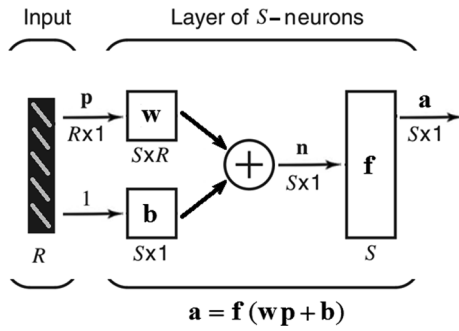


Fig. 4. A schematic view of the network consisting of S -neurons, R -inputs and one-layer network.

$$\xi(n) = \frac{1}{2} \sum_{j=1}^C e_j^2(n) \quad (21)$$

where C is the total number of neurons in the output layer of the network. The average squared error energy can be obtained by summing over all output n and then normalizing with respect to the size N as

$$\xi_{\text{avg}} = \frac{1}{N} \sum_{n=1}^N \xi(n) \quad (22)$$

The average squared error energy represents the objective function of the learning procedure that must be minimized due to changing the synaptic weights and bias coefficients. In order to minimize the objective function, an optimization algorithm must be employed. In the current study, the **Nelder-Mead** [39] method is employed as the optimization algorithm to evaluate the synaptic weight coefficients. It must be noted that although the gradient-based techniques, such as the Levenberg-Marquardt algorithm and gradient descent method, are more popular in conjunction with the ANN technique [40], it is observed here that a simplex algorithm, such as the Nelder-Mead method, is more efficient for the fracture mechanics problems studied in this research. Moreover, as the problem of the current study is a non-constraint one, the gradient-based approach consumes more computational costs in comparison with the simplex algorithm [41].

The ANN method typically commences with a training sample, where an optimization technique is used to obtain the synaptic weights of a multilayer perceptron (MLP) by encoding as many of the training examples as possible into the network. The aim is to design a generalized network, in which the input-output mapping computed by the ANN is nearly or exactly correct for the test data. The test data is a set of input data that is not used in creating or training the network. In the current study, 70% of data is utilized as the training dataset to simulate an appropriate model, and the remaining 30% is employed as the testing dataset to validate the developed model. Since there is a chaotic stress field near the crack tip region, a custom architecture with three hidden layers is implemented within the ANN algorithm, and the sigmoid, hyperbolic tangent and delta functions are employed as activation functions. These three functions are used to simulate all features of the stress field near the crack tip, such as the stress singularity. The hidden layers play a vital role in the operation of the MLP because they are employed as feature detectors. As the training (learning) process progresses, the hidden neurons start to gradually discover the salient features that specify the training data. This procedure is employed to nonlinearly transform the input data into a new space called the hidden space or feature space, in which the classes of interest in a pattern-classification duty, for instance, can be simply separated from each other than in the original input (loading) space. A schematic view of the proposed artificial neural network is presented in Fig. 5. The complementary information about the artificial neural networks and multilayer perceptron concepts can be found in [42].

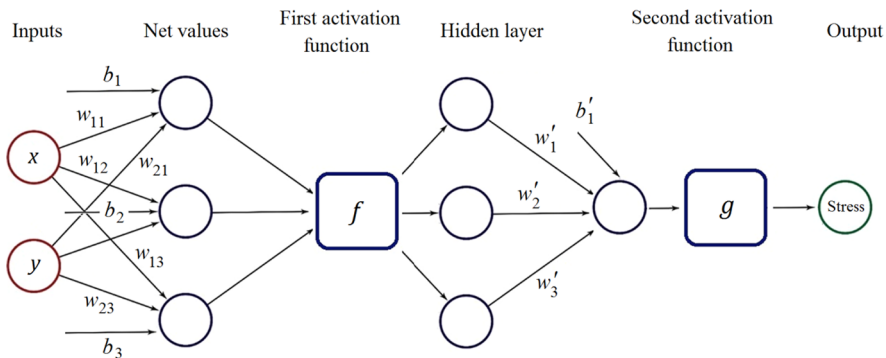


Fig. 5. A schematic view of the proposed Artificial Neural Network (ANN) technique.

4.2. Implementation of the ANN in stress recovery process

The capability of the ANN technique has been revealed extensively for the prediction of complex behavior in various problems. The artificial neural network is able to predict various stress fields according to their behavior; even so in regular nodal points that experience a uniform stress field, training the network with the Gauss points data in such a way produces a uniform stress field and recover the stress field appropriately. The ability of the ANN technique to model different behavior within a problem is one of the most important features of the artificial neural network that improves the recovered stress field in the adaptive finite element method. In Fig. 6, a schematic representation of the stress recovery is illustrated on a patch of elements at a singular point using the SPR and ANN techniques. It is obvious from Fig. 6(a) that the SPR polynomial function cannot improve the stress appropriately and

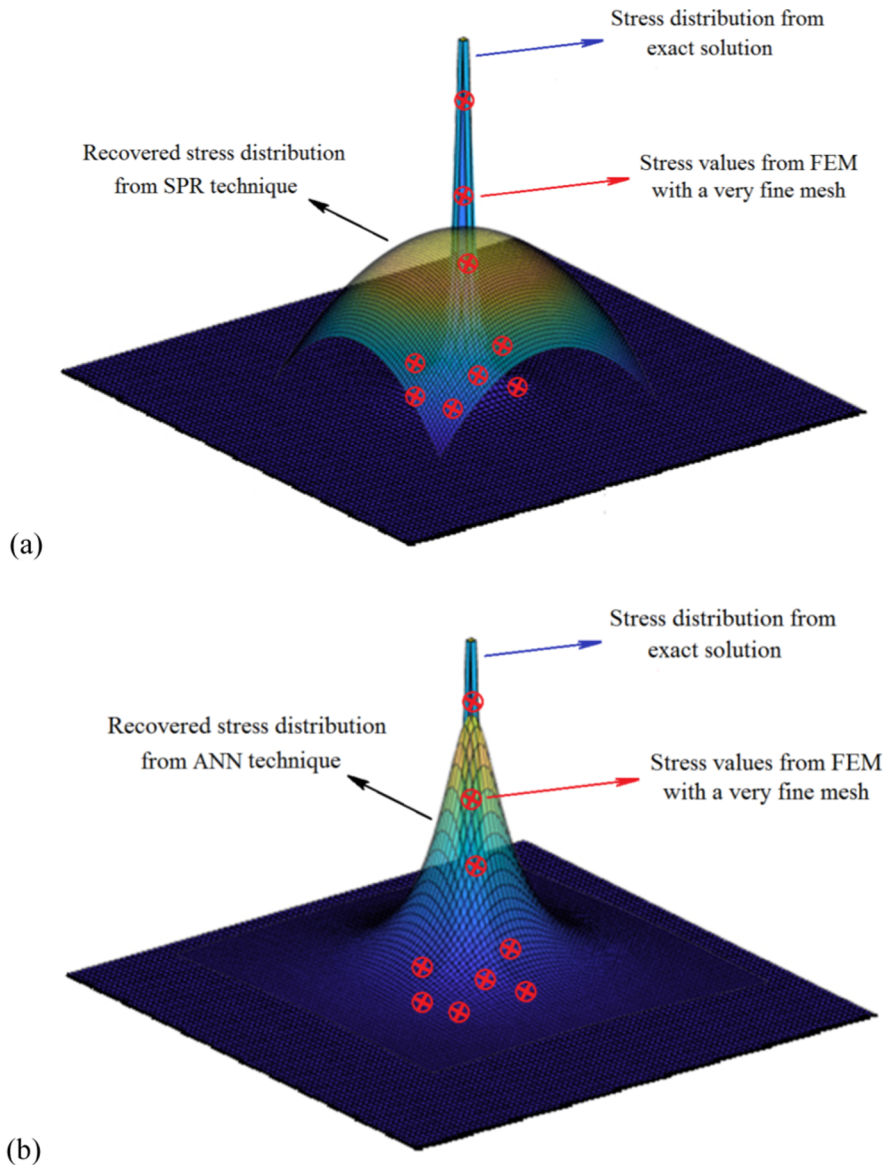


Fig. 6. The stress recovery on a patch of elements at a singular point; a) SPR method, b) ANN technique.

causes a large value of error in the stress field. However, the stress field can be improved by employing an artificial neural network and training the Gauss points data on a patch of elements, as shown in Fig. 6(b). In this study, the feed-forward back-propagation multilayer perceptron (MLP) neural network is employed.

In the ANN technique, a patch of elements is constructed surrounding each nodal point similar to the SPR method and the stress values of Gauss points on the patch are employed for training the corresponding neural network. The coordinates of Gauss points and corresponding stress values are specified in the network as input data and the stress function over the patch is obtained as the output of the network. A hidden layer of neurons is added to the network to model the singular behavior more appropriately. Since each component of the stress field (σ_x , σ_y , τ_{xy}) may represent different behavior, separate networks are employed for prediction of each stress component. As the ANN at each nodal point is trained separately, this network can be used efficiently to predict different behavior for various nodal points. According to Fig. 5, the output of each layer is obtained by applying the activation function to a combination of the input values of that layer. Hence, the output of hidden layer can be calculated as

$$h_i = f(w_{1i}x + w_{2i}y + b_i) \quad (23)$$

where h_i denotes the output of hidden layer, f is the activation function and, w_i and b_i represent the unknown weight and bias parameters, respectively. The activation function is usually a nonlinear sigmoid function that is applied to the weighted sum of inputs before the output passes to the next layer. The same procedure can be employed to generate the output layer where the output values of the hidden layer are taken as the input values of the output layer. The output of this layer leads to the final prediction of the recovered stress field as

$$\sigma_i = g(\sum w'_i f(w_{1i}x + w_{2i}y + b_i) + b'_i) \quad (24)$$

where g is the activation function of the output layer and, w'_i and b'_i are the unknown weight and bias parameters of the output layer. The recovered nodal stresses are obtained by replacing the nodal coordinates in Eq. (24). In this procedure, the weight and biases parameters are unknown and can be determined by training the network, in such a way that the predicted stress values result in a maximum coincidence with the Gauss points data on the patch. The error of the network is evaluated based on the difference between the predicted stress values at the Gauss points and those given directly by the finite element solution, i.e. $e_\sigma = \sigma_i - \hat{\sigma}$. The minimization of this error through the training process yields to the unknown parameters. During the training phase, the weight and biases parameters are successively modified according to the feed-forward back-propagation algorithm to reduce the estimated error. In the feed-forward neural network, connections do not form a cycle and the information is moved from the input layer, through the hidden layer and to the output layer. For back-propagation, the initial values of weight and biases parameters are usually set randomly, and are then altered according to the gradient descent rule iteratively. In this technique, the network calculates the derivative of the error function with respect to the network weights, and changes the weights such that the error decreases. The rate of change of the weight parameter can be obtained at iteration $n + 1$ as

$$\Delta w_{ij}(n+1) = \bar{\eta}(\bar{\delta}_j \sigma_i) + \alpha \Delta w_{ij}(n) \quad (25)$$

where $\bar{\eta}$ is the learning rate parameter, $\bar{\delta}_j$ is an index that indicates the rate of change of the error, and α is the momentum parameter. The learning rate parameter $\bar{\eta}$ exerts a powerful influence on the convergence process. If $\bar{\eta}$ is too small, then the training converges slowly. On the other hand, if $\bar{\eta}$ is too large, then the algorithm starts to oscillate and may even diverge. The momentum parameter α increases the size of the steps taken towards the minimization process by trying to jump from a local minimum. A small value of momentum parameter cannot reliably avoid the local minimum and can also slow down the training of the neural network. However, increasing the momentum parameter can be accompanied with the reduction of the learning rate. If both parameters are kept large, the global minimum may be missed through a huge step.

The initial values of weight and bias parameters in the training process have an important effect on the rate of convergence. Inappropriate selection of the initial parameters may change the slope of gradients slowly and training the network takes a large process of time. To overcome this drawback, the Nguyen-Wirdow initialization method [43] is employed here. In this technique, the parameters need to move in such a manner that the region of interest is divided into small intervals. Moreover, an interval is assigned to the weight and biases parameters at the beginning of the training process, in which the interval size and location can be adjusted during the training process. In Fig. 7, the flowchart of process sequences of the crack propagation simulation is presented on the basis of neural network method. It must be noted that the proposed ANN technique can be merely extended to three-dimensional FEM problems with minimum modifications. Since the number of variables, i.e. the nodal coordinates and stress components, increases in three-dimensional problems, the main objective is the definition of a proper structure of the artificial neural network to predict such more complicated simulation. The adjustment of the number of neurons, the number of hidden layers, and the activation functions play an important role in a successful stress recovery process.

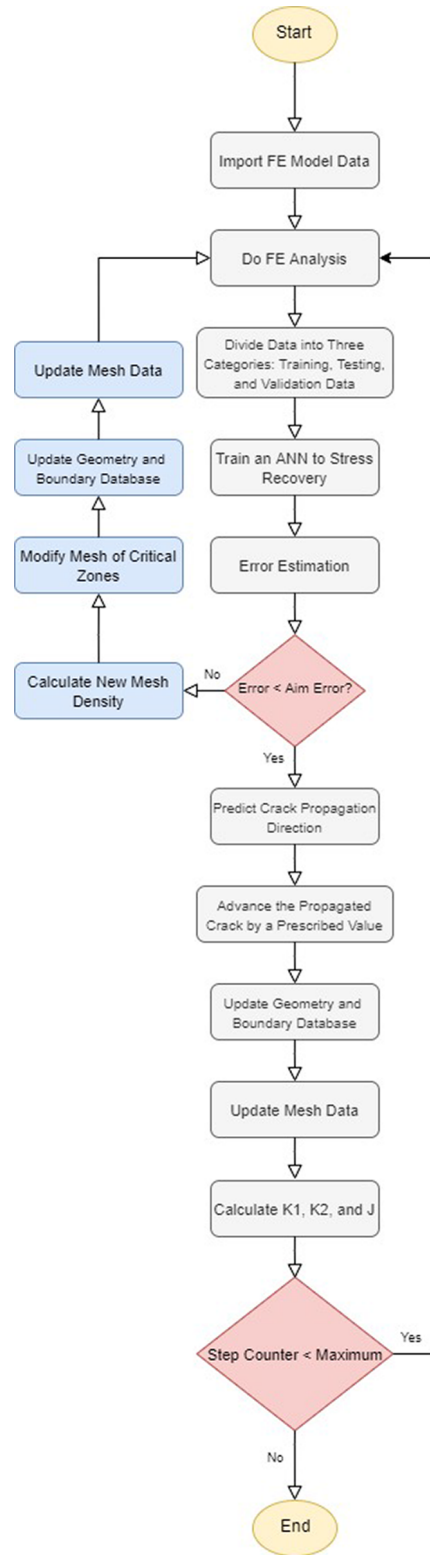


Fig. 7. The flowchart of process sequences of the crack propagation simulation on the basis of neural network method.

5. Numerical simulation results

In order to illustrate the accuracy and versatility of the proposed recovery technique in the framework of artificial neural network, several examples are solved numerically. Three examples are presented where the stress field is recovered using the averaging method, superconvergent patch recovery (SPR) technique, weighted superconvergent patch recovery (WSPR) method, and the artificial neural network (ANN) technique. In the finite element analysis, the six-noded triangular elements are used together with three Gauss quadrature points for the numerical integration. In all numerical examples, the behavior of material is assumed to be linearly elastic. The adaptive remeshing is initialized with a coarse uniform mesh and the adaptive meshes are generated based on the Zienkiewicz-Zhu error estimator. In artificial neural network algorithm, the symmetrical sigmoid function is used as the activation function to improve the training process particularly in the critical points of stress field, such as the crack tips, holes, etc. In order to evaluate the accuracy of the recovered stress field in the averaging, SPR, WSPR, and ANN techniques, a comparison is performed employing the FEM with a very fine mesh and the error of different techniques is estimated with respect to the fine FE mesh. The advantage of the ANN technique is illustrated over the conventional recovery techniques particularly in singular stress points.

5.1. Single edge notched beam with an eccentric crack

The first example is chosen to illustrate the performance of the proposed recovery technique for a simply supported beam with an eccentric crack. The beam is constructed from the asphalt concrete with the Young modulus of $E = 14.2\text{GPa}$ and the Poisson ratio of $\nu = 0.35$, as shown in Fig. 8. The problem is solved using the adaptive FEM strategy, in which the recovered stress fields are evaluated at the nodal points using the averaging, SPR, WSPR, and ANN algorithms, as described in Sections 3 and 4. It must be noted that the conventional stress recovery methods cannot result in the aim error of 5% at the first stage of adaptive remeshing, and the three successive mesh refinements are required to attain the predefined aim error, while the ANN method leads to the desired aim error at the first stage of adaptive mesh refinement. In the ANN algorithm, the stress fields of Gauss integration points are utilized for training the data, in which the training process is accomplished with the corresponding patch of elements. In Fig. 9, the adaptive mesh strategy is presented at different stages of crack propagation using the SPR and ANN techniques. Obviously, the ANN technique leads to the optimal mesh at the first stage of remeshing, while the SPR technique requires three successive mesh refinements to attain the aim error of 5 percent. Clearly, the efficiency of the proposed ANN method is obvious in this figure. In order to demonstrate the performance of the proposed computational algorithm, the three successive mesh refinements of the SPR technique are presented together with the first mesh refinement of the ANN technique in Fig. 10 for the aim error of 5 percent. In Fig. 11, the details of the training process in the ANN algorithm are illustrated including the fitting function of neural network and regression of the outputs and targets. In Fig. 12, the contours of recovered maximum principal stress are shown at the final stage of crack growth simulation. Since the exact solution is not available, the problem is solved using a very fine FE mesh. A comparison between the contours of the SPR and ANN recovery techniques and that obtained from the FEM with a very fine mesh illustrates that the proposed ANN algorithm results in more accurate recovered stress field, particularly at singular stress points of the beam.

In order to evaluate the accuracy of different recovery methods quantitatively, the recovered stress fields are obtained using

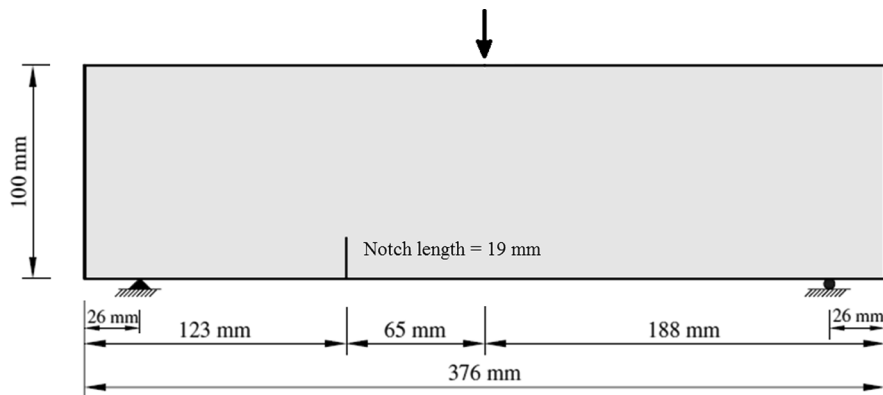


Fig. 8. A single edge notched beam with an eccentric crack; Geometry and boundary conditions.

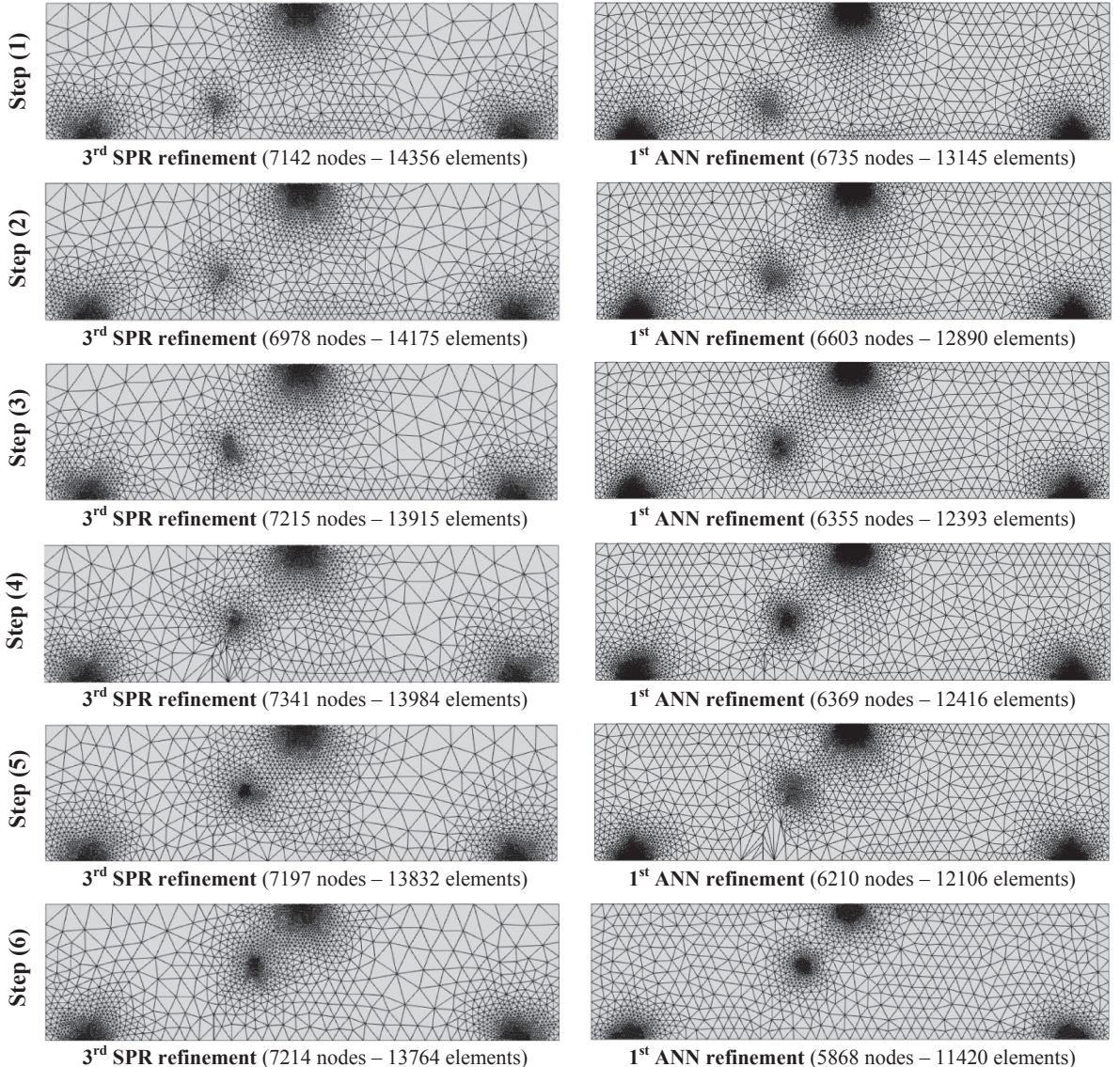


Fig. 9. A single edge notched beam with an eccentric crack; The adaptive mesh refinements obtained from the SPR and ANN techniques at different stages of crack propagation for the aim error of 5%

various techniques at the crack tip where the stress singularity occurs, and the results are summarized in Table 1. Moreover, a very fine FE mesh is employed as an approximation of the exact stress field to estimate the error on the basis of difference between the recovered solution and that obtained from the finite element analysis with very fine mesh. The details of all mesh refinements are given in Table 2. Clearly, the performance of the ANN technique can be observed from the estimated error of various approaches in Tables 1 and 2. In fact, the conventional recovery methods utilize the fitting procedure based on a polynomial function passed through the stress values of Gauss integration points that underestimate the recovered stress field. However, the ANN technique

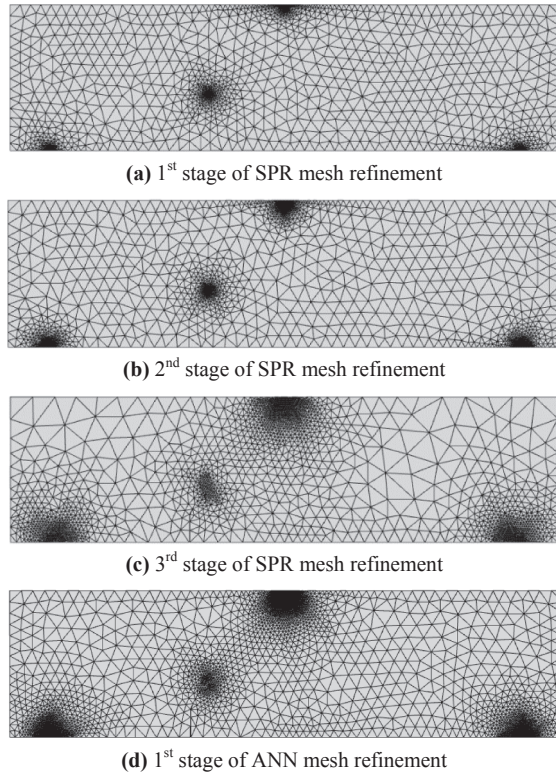


Fig. 10. Adaptive mesh refinement in a single edge notched beam with an eccentric crack for the aim error of 5%; (a–c) three successive mesh refinements using the SPR technique, (d) the 1st mesh refinement using the ANN technique.

evaluates the recovered stress field by training the data obtained from the stress values of Gauss integration points at the crack tip region. In Fig. 13, the evolutions of recovered stress are plotted on the patch of elements at the crack tip region using different recovery techniques at the final stage of crack propagation. It can be seen from this figure that the averaging method leads to a rough approximation of the recovered stress field; while the SPR and WSPR methods improve the recovered stress field reasonably, the proposed ANN algorithm is capable to capture the singular stress field at the crack tip region properly.

In order to demonstrate the crack propagation trajectory, the maximum circumferential stress criterion is employed to determine the crack growth direction. In this manner, the crack propagates with a predefined constant length at each step of crack propagation. In Fig. 14, a comparison is performed between the crack trajectories obtained from the SPR and ANN techniques and that of the FEM with a very fine mesh. A good agreement can be seen between the crack trajectory of the ANN method and that obtained from the fine FE mesh. The evolutions of J -integral with the crack length are plotted in Fig. 15 using different recovery techniques. Also plotted in Fig. 16 are the evolutions of mode-I and mode-II stress intensity factors (K_I and K_{II}) with the crack length using different recovery methods. A comparison between the results of J -integral, K_I and K_{II} obtained from the ANN method and those obtained from the FEM analysis with a very fine mesh illustrates the performance of ANN method over the conventional recovery techniques particularly at singular stress points.

5.2. A plate with two holes and multiple cracks

The next example is chosen to illustrate the capability of the proposed ANN algorithm in a more challenging problem. In this example, a rectangular plate with two circular holes and multiple cracks is subjected to a prescribed displacement at the top edge, as

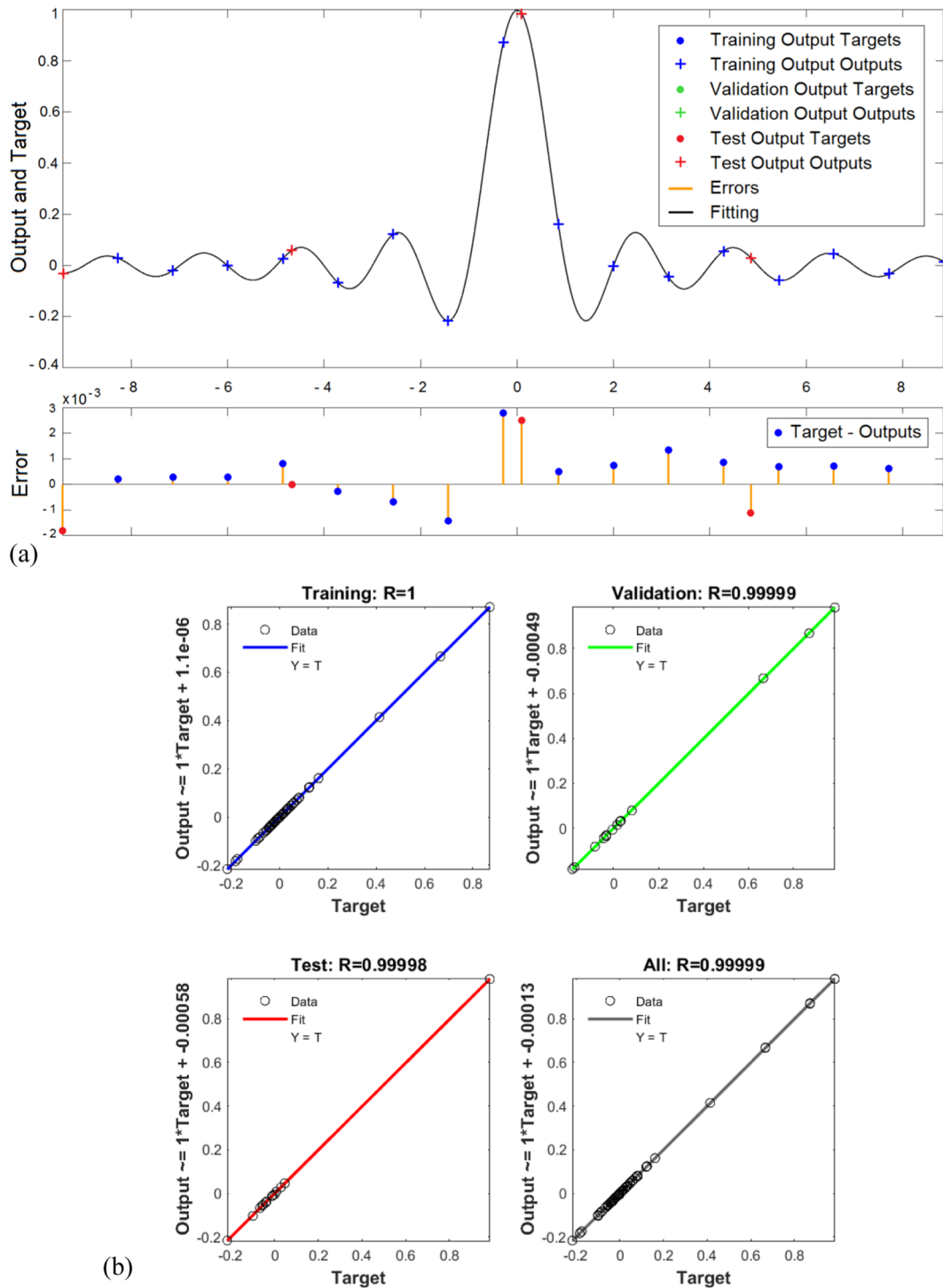


Fig. 11. The details of the neural network training; (a) the predicted function of stress field at the crack tip, (b) the regression of the outputs and targets.

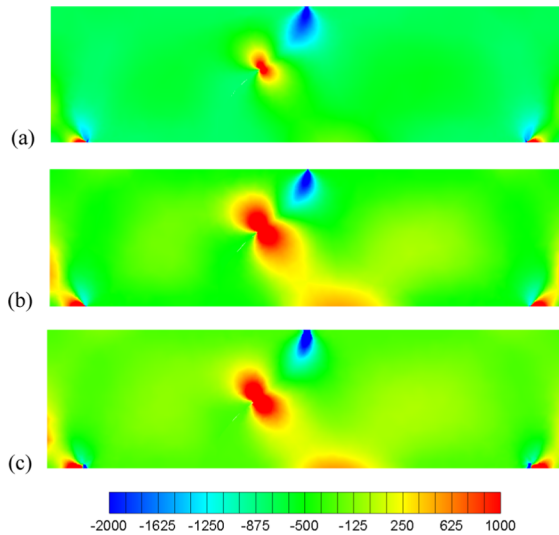


Fig. 12. A single edge notched beam with an eccentric crack; The contours of recovered maximum principal stress at the final stage of crack growth using: (a) SPR technique, (b) ANN technique, (c) FEM with a very fine mesh.

Table 1

A single edge notched beam with an eccentric crack; The estimated error of different recovery techniques at crack tip nodal point.

| Recovery technique | Stress σ_x | Stress σ_y | Stress τ_{xy} | Error of stress σ_x (%) | Error of stress σ_y (%) | Error of stress τ_{xy} (%) |
|----------------------|-------------------|-------------------|--------------------|--------------------------------|--------------------------------|---------------------------------|
| averaging | 3938.20 | 1979.49 | -1300.66 | 51.69 | 59.13 | 27.22 |
| SPR (1st remeshing) | 6952.37 | 4164.33 | -1563.53 | 14.72 | 14.01 | 12.51 |
| SPR (2nd remeshing) | 7417.36 | 4277.64 | -1609.71 | 9.02 | 11.67 | 9.92 |
| SPR (3rd remeshing) | 7614.23 | 4467.51 | -1697.85 | 6.60 | 7.75 | 4.99 |
| WSPR | 7256.99 | 4232.81 | -1595.64 | 10.98 | 12.60 | 10.71 |
| ANN | 7826.08 | 4537.40 | -1726.09 | 4.00 | 6.31 | 3.41 |
| FEM with a fine mesh | 8152.38 | 4843.03 | -1787.01 | 0.00 | 0.00 | 0.00 |

Table 2

A single edge notched beam with an eccentric crack; The details of mesh refinements.

| | SPR (1st remehing) | | SPR (2nd remehing) | | SPR (3rd remehing) | | ANN | | FEM with a fine mesh | |
|--------|--------------------|--------------|--------------------|--------------|--------------------|--------------|-----------|--------------|----------------------|--------------|
| | No. Nodes | No. Elements | No. Nodes | No. Elements | No. Nodes | No. Elements | No. Nodes | No. Elements | No. Nodes | No. Elements |
| Step 1 | 4158 | 7846 | 5410 | 9568 | 7142 | 14,356 | 6735 | 13,145 | 14,635 | 20,163 |
| Step 2 | 3876 | 7793 | 4414 | 9575 | 6978 | 14,175 | 6603 | 12,890 | 15,124 | 21,365 |
| Step 3 | 3971 | 7834 | 4376 | 9494 | 7215 | 13,915 | 6355 | 12,393 | 15,284 | 20,411 |
| Step 4 | 4017 | 7412 | 5430 | 8602 | 7341 | 13,984 | 6369 | 12,416 | 14,938 | 20,745 |
| Step 5 | 4096 | 7486 | 5401 | 8545 | 7197 | 13,832 | 6210 | 12,106 | 16,023 | 21,461 |
| Step 6 | 4135 | 7338 | 5052 | 7975 | 7214 | 13,764 | 5868 | 11,420 | 16,231 | 21,214 |

shown in Fig. 17. The material properties of the plate is as follows; the Young modulus of $E = 20\text{GPa}$ and the Poisson ratio of $\nu = 0.3$. This problem was studied by Shiralinezhad and Moslemi [44] to present the capability of their mesh partitioning technique in multiple crack problems. In Fig. 18, the adaptive mesh refinements are presented at different stages of crack propagation in the third stage of SPR refinement and first stage of ANN refinement for the aim error of 5%. Also presented in Fig. 19 are the three successive

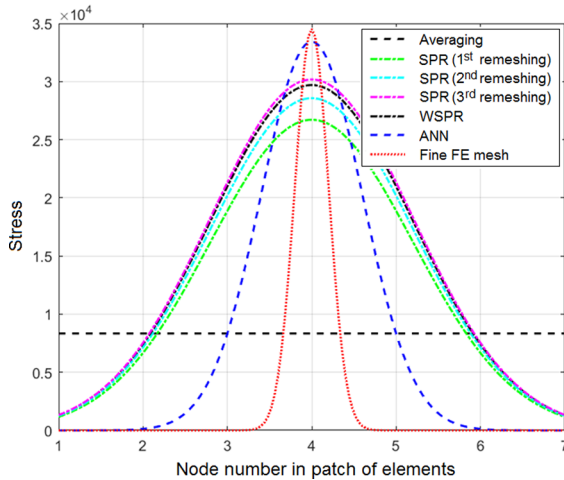


Fig. 13. A beam with an eccentric crack; The evolutions of recovered stresses on the patch of elements at the crack tip using different recovery techniques at the final stage of crack propagation.

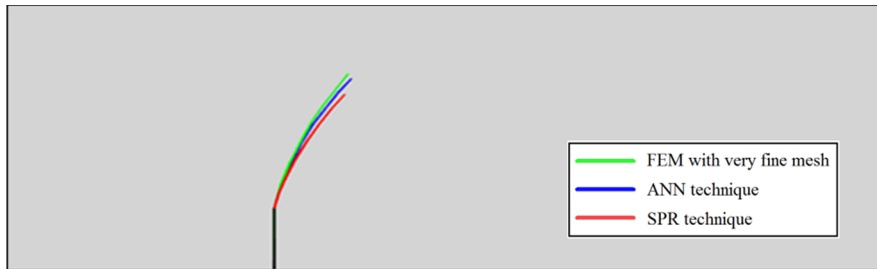


Fig. 14. A single edge notched beam with an eccentric crack; A comparison between the crack trajectories obtained from the SPR and ANN techniques and that of the FEM with a very fine mesh.

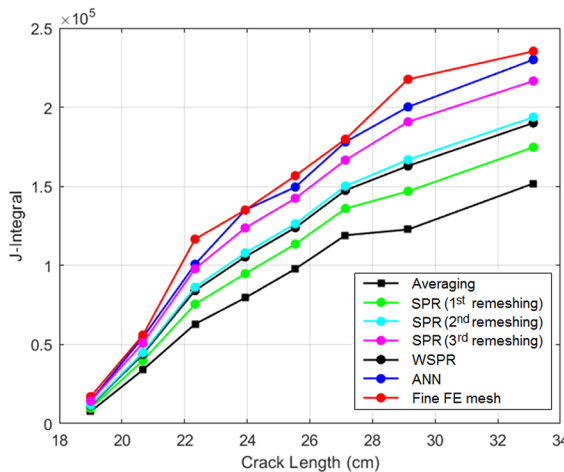


Fig. 15. A single edge notched beam with an eccentric crack; The evolutions of J -integral with the crack length using different recovery techniques.

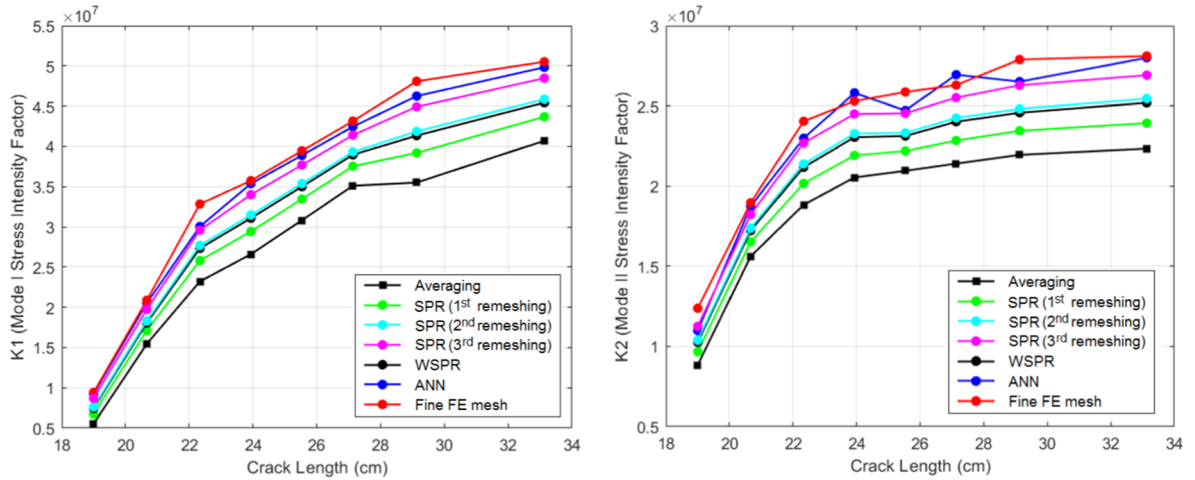


Fig. 16. A single edge notched beam with an eccentric crack; The evolutions of mode-I and mode-II stress intensity factors (K_I and K_{II}) with the crack length using different recovery methods.

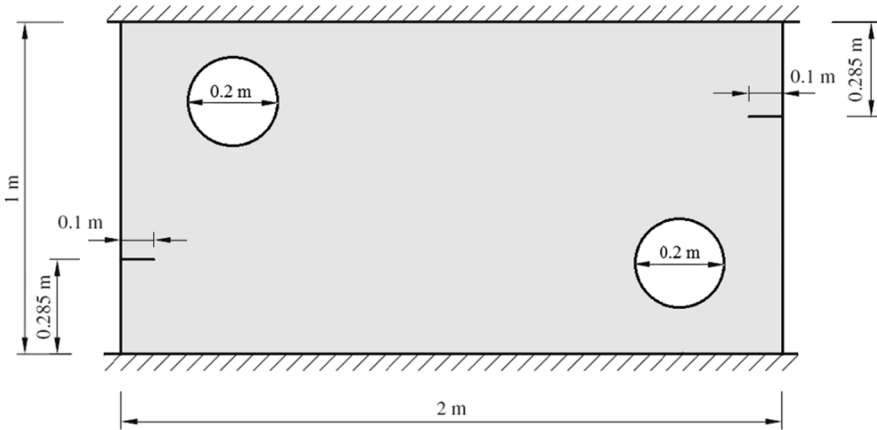


Fig. 17. A plate with two holes and multiple cracks; Geometry and boundary conditions.

mesh refinements of the SPR technique together with the first mesh refinement of the ANN technique for the aim error of 5 percent that illustrates the efficiently of the proposed ANN method. The contours of recovered maximum principal stress are shown in Fig. 20 at the final stage of crack growth. Clearly, the recovered stress distribution provided by the ANN method is in a good agreement with that obtained from the fine FE mesh. Moreover, the accuracy of different recovery methods is obtained quantitatively by estimating the error of recovered stress fields using various techniques at the crack tip, as given in Table 3. The details of all mesh refinements are given in Table 4. In Fig. 21, the evolutions of recovered stress are plotted on the patch of elements at the crack tip region using different recovery techniques at the final stage of crack propagation. It can be seen from this figure that the ANN method can be used efficiently to capture the singular stress field at the crack tip region. In Fig. 22, a comparison is performed between the crack trajectories obtained from the SPR and ANN techniques and that of the FEM with a very fine mesh. The symmetrical crack trajectory of the specimen is obvious in this figure. A good agreement can also be seen between the crack trajectory of the ANN method and that obtained from the fine FE mesh. The evolutions of J -integral with the crack length are plotted in Fig. 23 using different recovery techniques. Finally, the evolutions of mode-I and mode-II stress intensity factors (K_I and K_{II}) are plotted with the crack length in

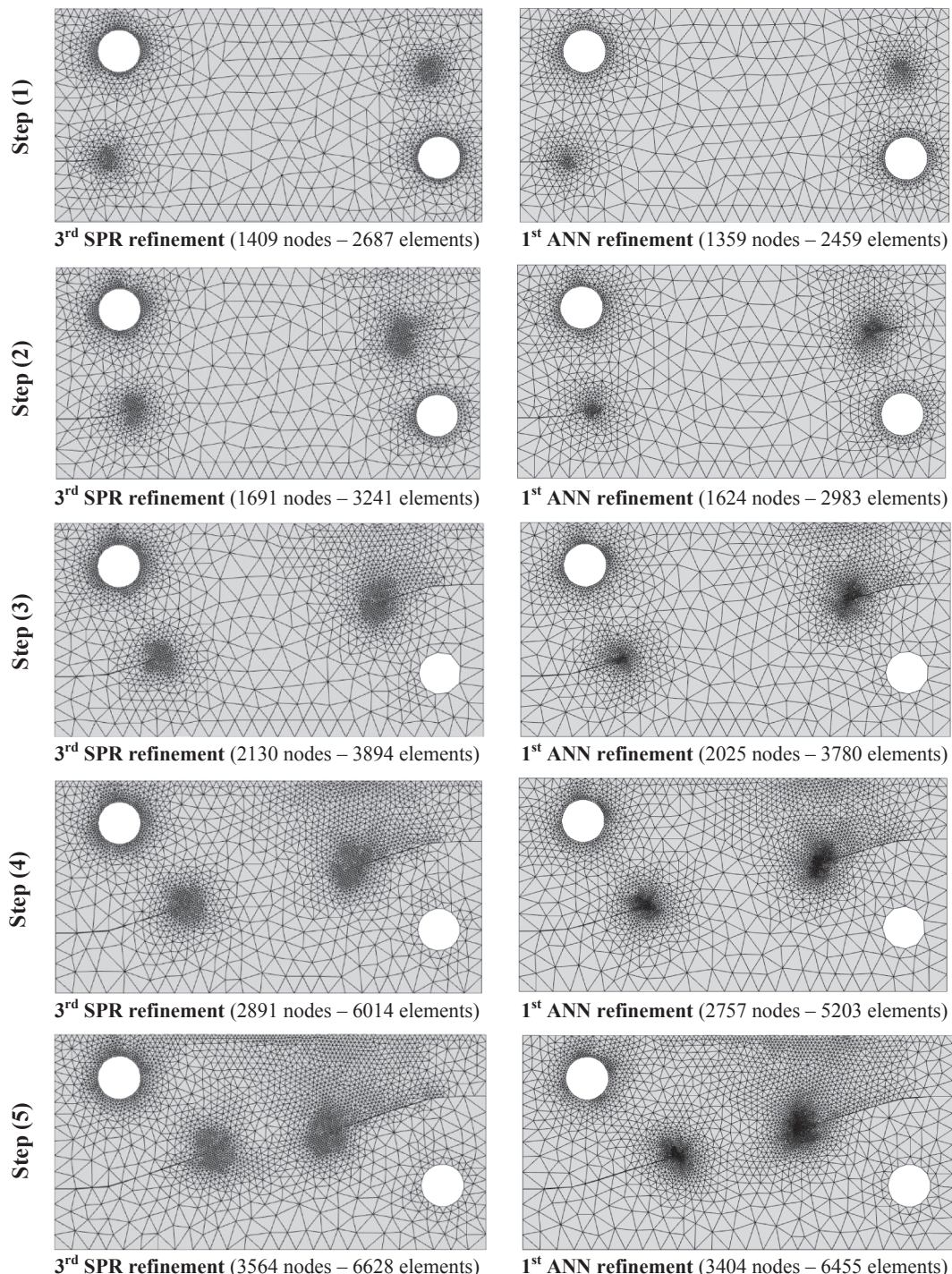


Fig. 18. A plate with two holes and multiple cracks; The adaptive mesh refinements obtained from the SPR and ANN techniques at different stages of crack propagation for the aim error of 5%

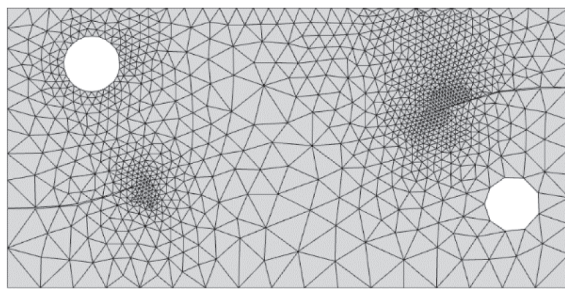
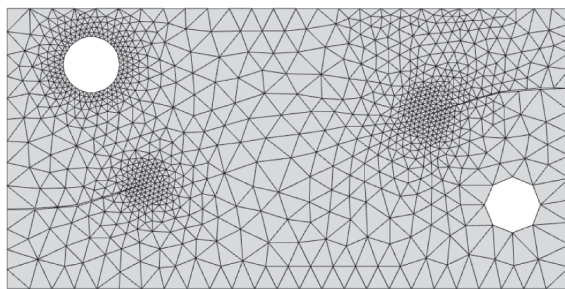
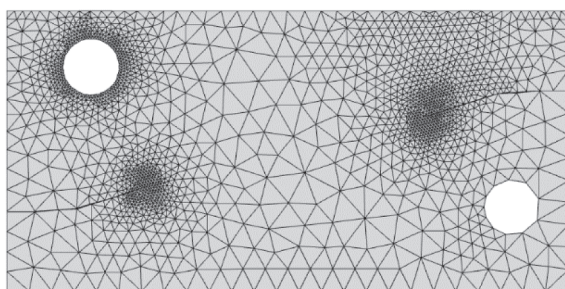
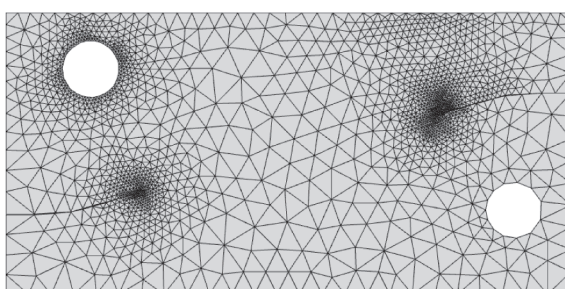
(a) 1st stage of SPR mesh refinement(b) 2nd stage of SPR mesh refinement(c) 3rd stage of SPR mesh refinement(d) 1st stage of ANN mesh refinement

Fig. 19. Adaptive mesh refinement in a plate with two holes and multiple cracks for the aim error of 5%; (a–c) three successive mesh refinements using the SPR technique, (d) the 1st mesh refinement using the ANN technique.

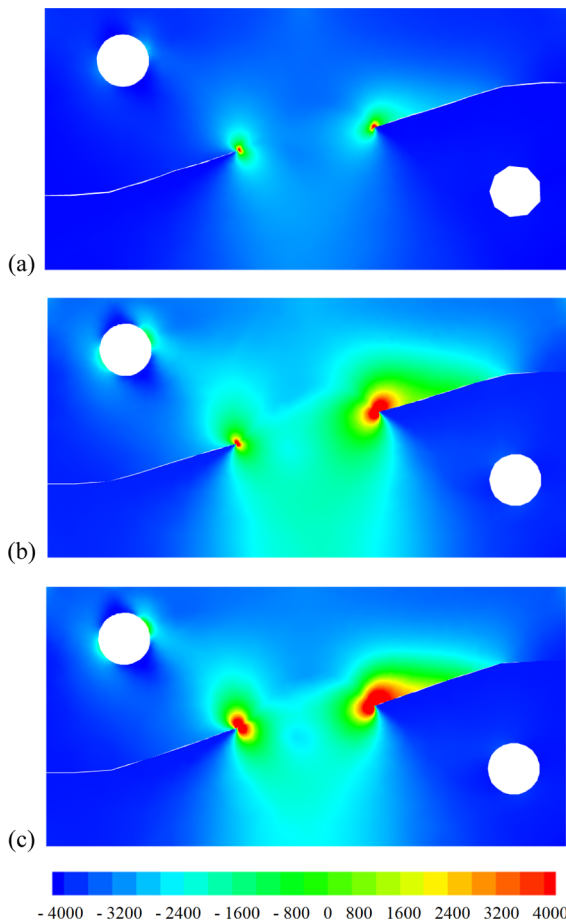


Fig. 20. A plate with two holes and multiple cracks; The contours of recovered maximum principal stress at the final stage of crack growth using; (a) SPR technique, (b) ANN technique, (c) FEM with a very fine mesh.

Table 3

A plate with two holes and multiple cracks; The estimated error of different recovery techniques at crack tip nodal point of the right hole.

| Recovery technique | Stress σ_x | Stress σ_y | Stress τ_{xy} | Error of stress σ_x (%) | Error of stress σ_y (%) | Error of stress τ_{xy} (%) |
|----------------------|-------------------|-------------------|--------------------|--------------------------------|--------------------------------|---------------------------------|
| averaging | 635168.9 | 1296363.2 | 59708.5 | 61.93 | 58.55 | 37.00 |
| SPR (1st remeshing) | 1294772.7 | 2496071.7 | 76284.1 | 22.40 | 20.19 | 19.51 |
| SPR (2nd remeshing) | 1469742.02 | 2785864.75 | 84280.54 | 11.91 | 10.92 | 11.08 |
| SPR (3rd remeshing) | 1540721.57 | 2970921.39 | 88641.51 | 7.66 | 5.00 | 6.48 |
| WSPR | 1399754.3 | 2634156.9 | 82361.9 | 16.11 | 15.77 | 13.10 |
| ANN | 1567754.2 | 3012295.6 | 90434.6 | 6.04 | 3.68 | 4.59 |
| FEM with a fine mesh | 1668465.8 | 3127415.6 | 94780.3 | 0.00 | 0.00 | 0.00 |

Table 4

A plate with two holes and multiple cracks; The details of mesh refinements.

| | SPR (1st remeshing) | | SPR (2nd remeshing) | | SPR (3rd remeshing) | | ANN | | FEM with a fine mesh | |
|---------------|---------------------|--------------|---------------------|--------------|---------------------|--------------|-----------|--------------|----------------------|--------------|
| | No. Nodes | No. Elements | No. Nodes | No. Elements | No. Nodes | No. Elements | No. Nodes | No. Elements | No. Nodes | No. Elements |
| Step 1 | 678 | 1271 | 834 | 1730 | 1409 | 2687 | 1359 | 2459 | 9137 | 14,672 |
| Step 2 | 764 | 1304 | 1292 | 2142 | 1691 | 3241 | 1624 | 2983 | 9279 | 14,935 |
| Step 3 | 791 | 1319 | 1637 | 3229 | 2130 | 3894 | 2025 | 3780 | 9698 | 15,042 |
| Step 4 | 824 | 1397 | 2419 | 3814 | 2891 | 6014 | 2757 | 5203 | 9742 | 15,034 |
| Step 5 | 853 | 1468 | 2877 | 4986 | 3564 | 6628 | 3404 | 6455 | 10,219 | 14,962 |

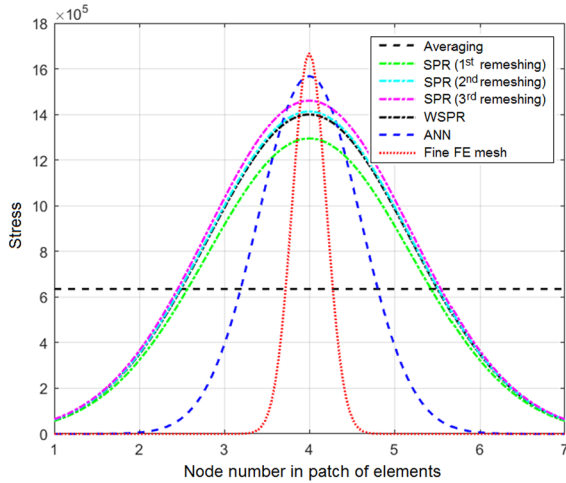


Fig. 21. A plate with two holes and multiple cracks; The evolutions of recovered stresses on the patch of elements at the crack tip using different recovery methods at final stage of crack propagation.

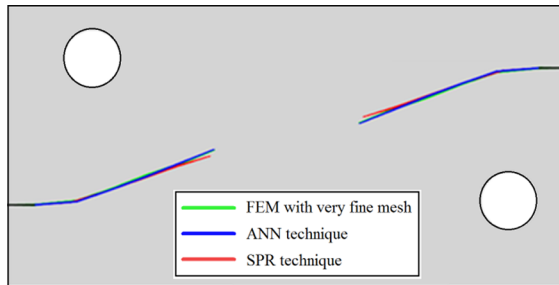


Fig. 22. A plate with two holes and multiple cracks; A comparison between the crack trajectories obtained from the SPR and ANN techniques and that of the FEM with a very fine mesh.

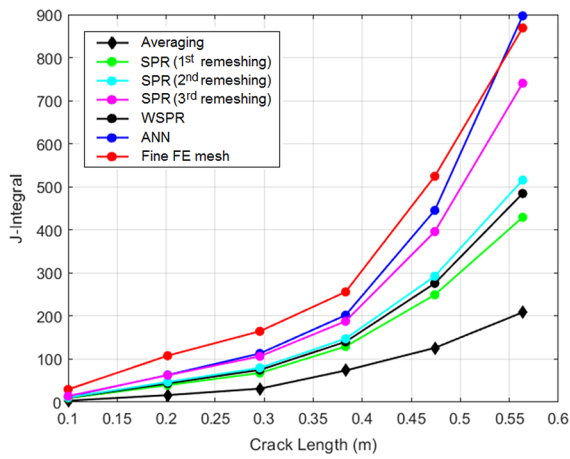


Fig. 23. A plate with two holes and multiple cracks; The evolutions of J -integral with the crack length using different recovery techniques.

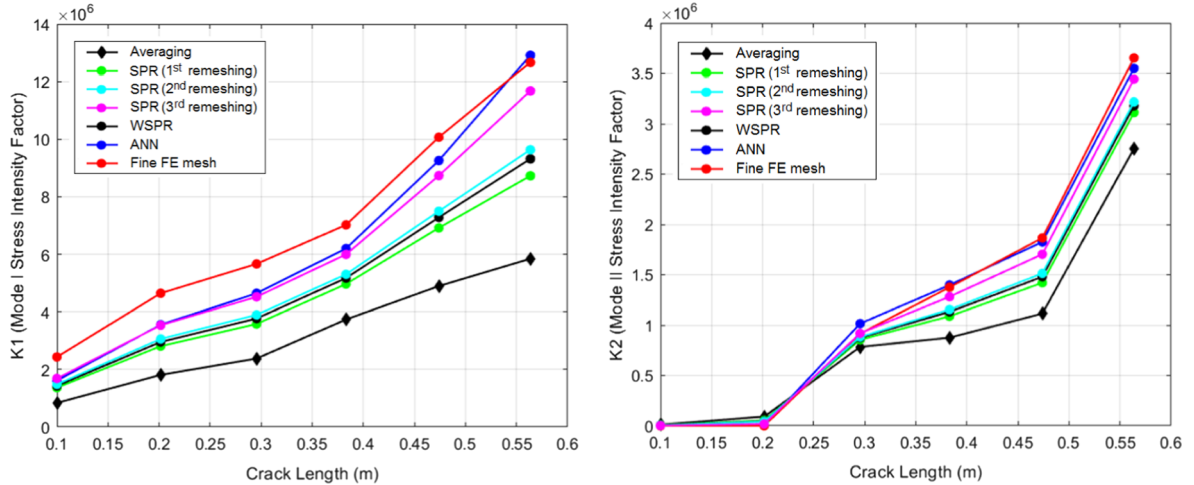


Fig. 24. A plate with two holes and multiple cracks; The evolutions of mode-I and mode-II stress intensity factors (K_I and K_{II}) with the crack length using different recovery techniques.

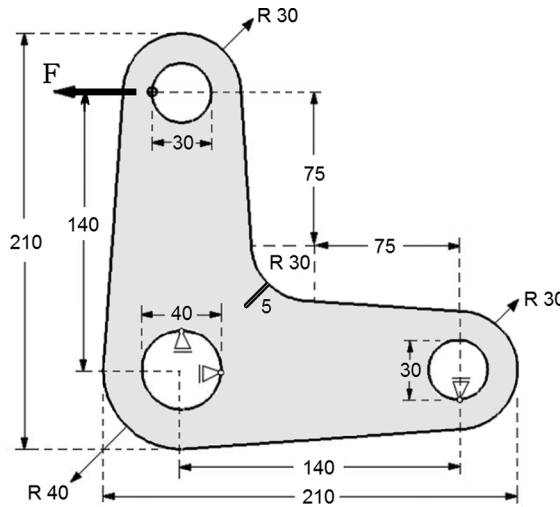


Fig. 25. The knee-lever with a corner crack; Geometry and boundary conditions (all dimensions in mm).

Fig. 24 using different recovery methods. These figures clearly demonstrate the performance of ANN method over the conventional recovery techniques particularly in singular stress points.

5.3. A knee-lever with a corner crack

The last example is a practical engineering problem chosen to illustrate the performance of the proposed computational algorithm by modeling a knee-lever connection that is extensively used in mechanical systems. The knee-lever has an initial crack in the symmetric plane oriented with the angle of 45°, as shown in Fig. 25. The specimen is made of aluminum alloy AlZnMgCu because of its excellent ratio of the strength to density. The aluminum alloy properties are chosen as follows; the Young modulus $E = 70.6\text{GPa}$

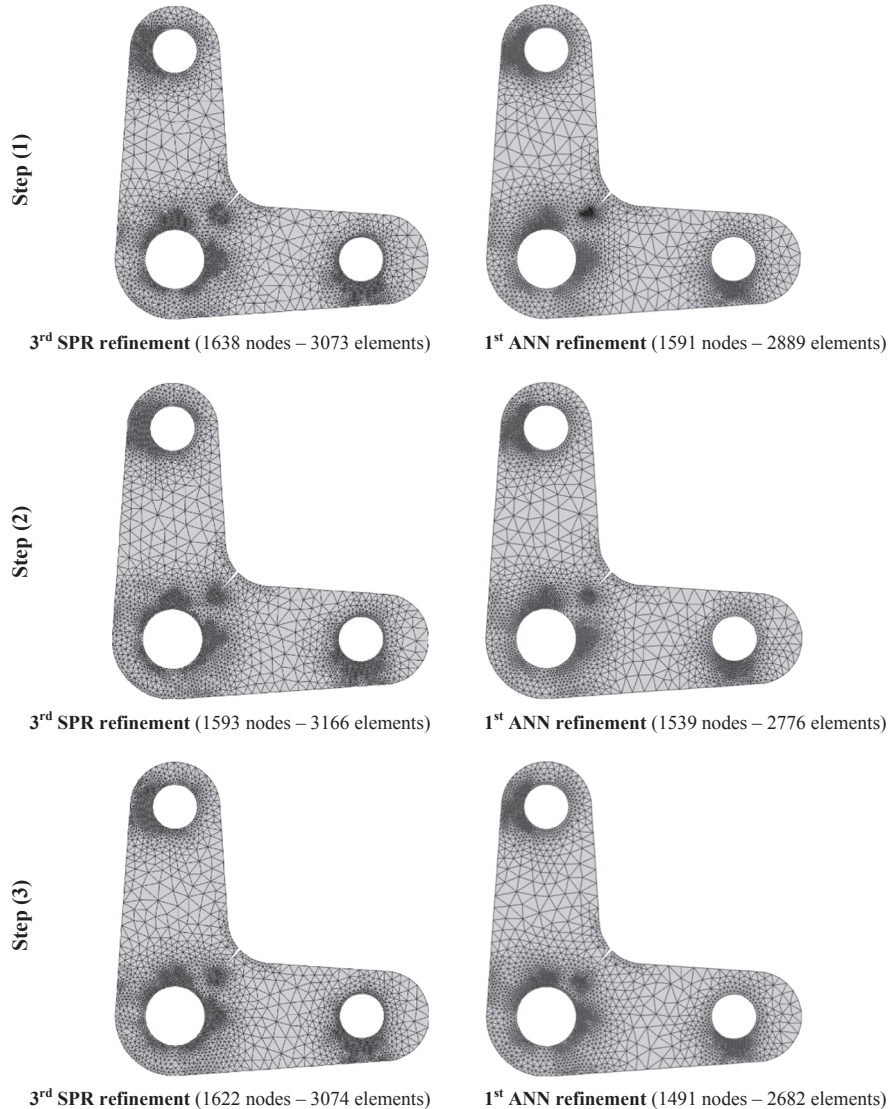


Fig. 26. The knee-lever with a corner crack; The adaptive mesh refinements obtained from the SPR and ANN techniques at different stages of crack propagation for the aim error of 5%

and the Poisson ratio $\nu = 0.34$. The component is subjected to a horizontal loading $7kN$ at the upper hole. The numerical modeling is performed to investigate the accuracy of different recovery schemes and their performances. The symmetric loading of the component leads to the mode I crack propagation. In Fig. 26, the adaptive mesh refinements are presented using the SPR and ANN techniques at different stages of crack propagation. The process of three successive mesh refinements in the SPR technique is presented in Fig. 27 along with the first mesh refinement in the ANN method. It is obvious that the SPR technique leads to an optimal mesh for the aim error of 5% with high computational costs in three stages of mesh refinements. In Fig. 28, the contours of recovered maximum principal stress are shown at the final stage of crack growth. Obviously, the recovered stress distribution obtained by the ANN method is in a good agreement with that obtained from the fine FE mesh. Furthermore, the accuracy of different recovery

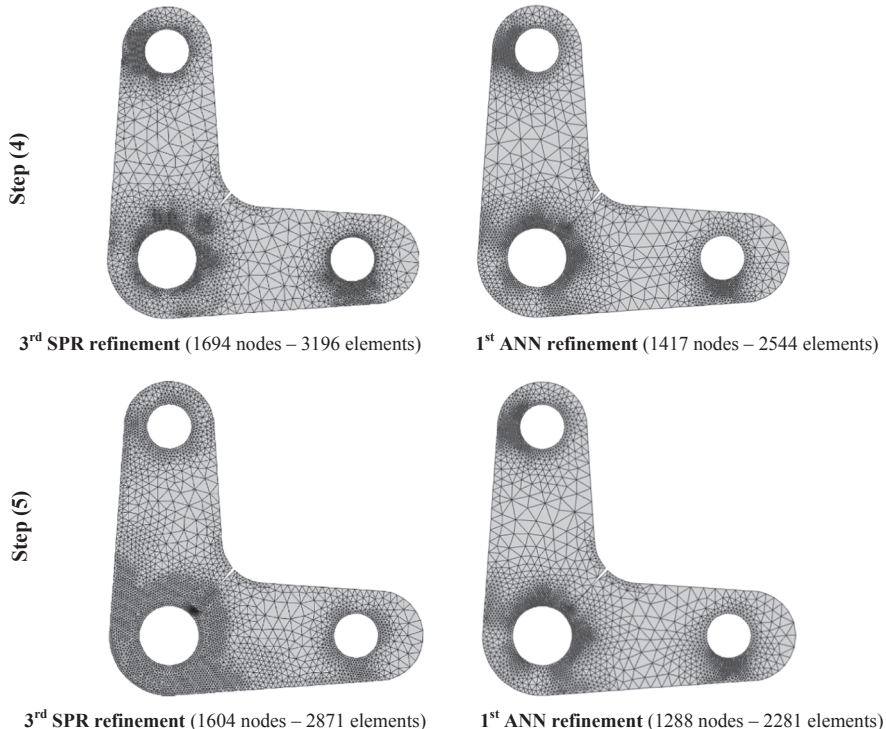


Fig. 26. (continued)

techniques is investigated quantitatively by estimating the error of recovered stress field using various techniques at the crack tip, as presented in Table 5. In order to demonstrate the computational costs of two methods, the number of nodes and elements during the mesh refinements are summarized in Table 6 for the SPR and ANN techniques. In Fig. 29, the evolutions of recovered stress are plotted on the patch of elements at the crack tip region using different recovery techniques at the final stage of crack propagation. Clearly, it can be seen from this figure that the ANN method can be used properly to capture the singular stress field at the crack tip region. In Fig. 30, a comparison is performed between the crack trajectories obtained from the SPR and ANN techniques and that of the FEM with a very fine mesh. A good agreement can be seen between the crack trajectory of the ANN method and that obtained from the fine FE mesh. The evolutions of J -integral with the crack length are plotted in Fig. 31 using different recovery techniques. Finally, the evolutions of mode-I and mode-II stress intensity factors (K_I and K_{II}) with the crack length are plotted in Fig. 32 using various recovery methods. This practical example clearly represents the performance of ANN technique in capturing the singular stress fields over the conventional recovery techniques.

6. Conclusion

In the present paper, an efficient stress recovery technique was presented in adaptive finite element method based on the artificial neural network algorithm. The technique relies on a feed-forward back-propagation multilayer perceptron neural network to improve the accuracy of the recovered stress field. Various exclusive networks were constructed for each nodal point that were trained according to the stress component of Gauss integration points on the patch of elements containing the target nodal point. In artificial neural network algorithm, the symmetrical sigmoid function was employed as the activation function to improve the training process particularly in the singular stress fields. The main advantage of the ANN method is its capability to recover the stress field more efficient than the conventional recovery techniques particularly in the regions with a high stress gradient where the conventional techniques are not able to improve the stress values efficiently. It was shown that the conventional stress recovery methods cannot

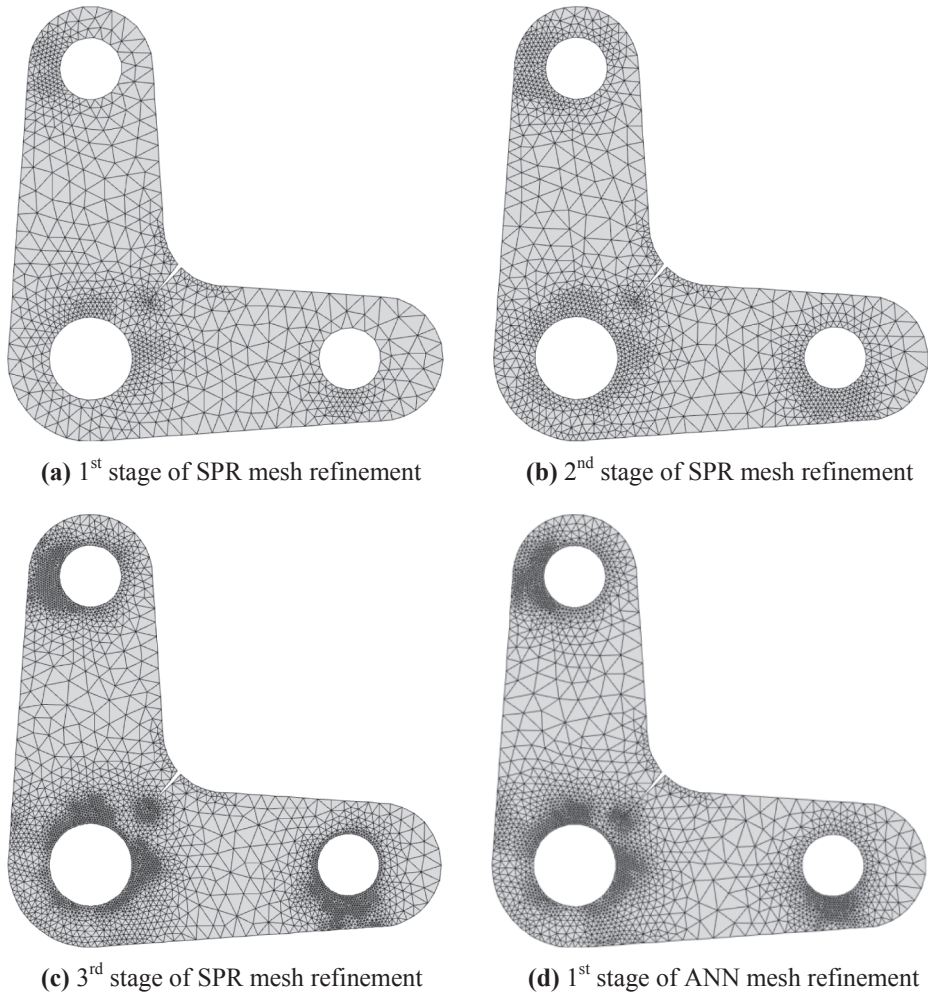


Fig. 27. Adaptive mesh refinement in the knee-lever with a corner crack for the aim error of 5%; (a–c) three successive mesh refinements using the SPR technique, (d) the 1st mesh refinement using the ANN technique.

result in the desired aim error at the first stage of adaptive remeshing, and several successive mesh refinements are required to attain the predefined aim error, while the ANN method leads to the desired aim error at the first stage of adaptive mesh refinement. Finally, three numerical examples modeled to demonstrate the efficiency and accuracy of the proposed computational algorithm, including a single edge notched beam with an eccentric crack, a rectangular plate with two circular holes and multiple cracks, and a knee-lever with a corner crack. For each example, a very fine FE mesh was employed as an approximation of the exact stress field to estimate the error of stress field on the basis of difference between the recovered solution and that obtained from the finite element analysis with a very fine mesh. In order to evaluate the accuracy of the proposed recovery technique, the results of ANN method were compared with the conventional recovery methods, including the averaging method, superconvergent patch recovery (SPR) technique, and weighted superconvergent patch recovery (WSPR) method. It was shown that the artificial neural network can be used accurately to recover the stress field particularly at the singular points. In a later research work, the proposed ANN technique will be extended to three-dimensional FEM problems, in which the main challenge is the construction of a proper structure for the artificial neural network with more relevant parameters in 3D space. This may include the determination of the number of the neurons, number of hidden layers, and activation functions that play an important role in a successful stress recovery process.

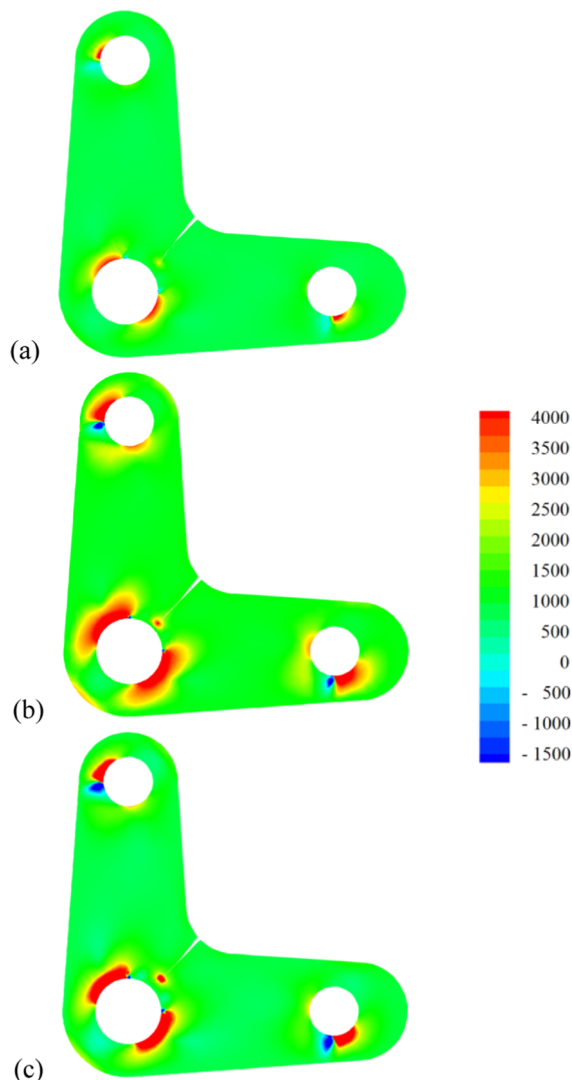


Fig. 28. The knee-lever with a corner crack; The contours of recovered maximum principal stress at the final stage of crack growth using; (a) SPR technique, (b) ANN technique, (c) FEM with a very fine mesh.

Table 5

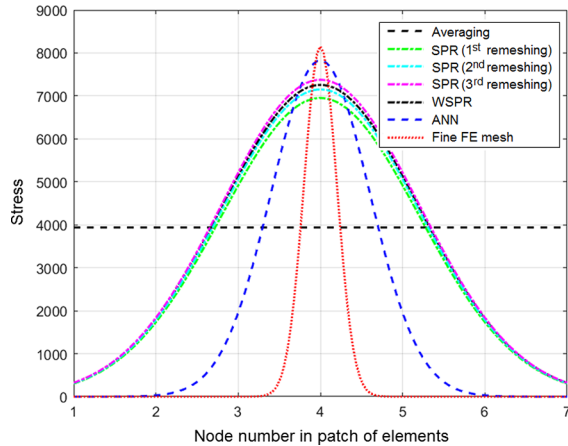
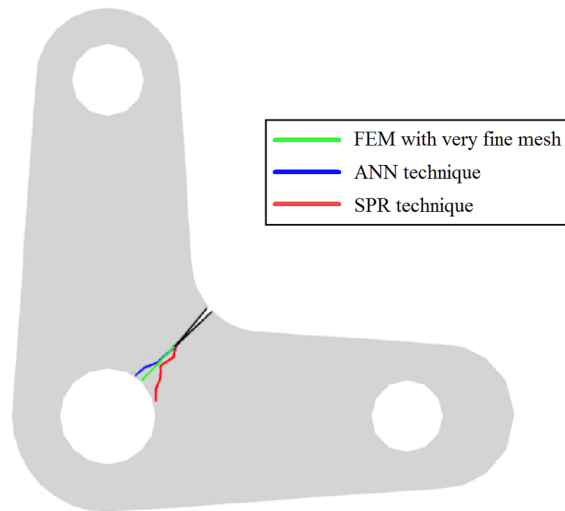
A knee-lever with a corner crack; The estimated error of different recovery techniques at crack tip nodal point.

| Recovery technique | Stress σ_x | Stress σ_y | Stress τ_{xy} | Error of stress σ_x (%) | Error of stress σ_y (%) | Error of stress τ_{xy} (%) |
|----------------------|-------------------|-------------------|--------------------|--------------------------------|--------------------------------|---------------------------------|
| averaging | 8342.61 | 8206.40 | -1749.21 | 75.84 | 76.45 | 75.20 |
| SPR (1st remeshing) | 26715.13 | 26781.33 | -5247.44 | 22.62 | 23.13 | 25.60 |
| SPR (2nd remeshing) | 31187.79 | 31251.31 | -6333.00 | 9.67 | 10.31 | 10.21 |
| SPR (3rd remeshing) | 32529.20 | 32694.13 | -6627.25 | 5.78 | 6.16 | 6.04 |
| WSPR | 29702.66 | 29763.15 | -6031.43 | 13.97 | 14.58 | 14.49 |
| ANN | 33432.17 | 33746.53 | -6615.72 | 3.17 | 3.14 | 6.20 |
| FEM with a fine mesh | 34525.66 | 34841.92 | -7053.10 | 0.00 | 0.00 | 0.00 |

Table 6

A knee-lever with a corner crack; The details of mesh refinements.

| SPR (1st remeshing) | | SPR (2nd remeshing) | | SPR (3rd remeshing) | | ANN | | FEM with a fine mesh | |
|---------------------|--------------|---------------------|--------------|---------------------|--------------|-----------|--------------|----------------------|--------------|
| No. Nodes | No. Elements | No. Nodes | No. Elements | No. Nodes | No. Elements | No. Nodes | No. Elements | No. Nodes | No. Elements |
| Step 1 | 625 | 1672 | 1139 | 2274 | 1638 | 3073 | 1591 | 2889 | 10,485 |
| Step 2 | 697 | 1596 | 1124 | 2196 | 1593 | 3166 | 1539 | 2776 | 10,314 |
| Step 3 | 689 | 1617 | 1197 | 2214 | 1622 | 3074 | 1491 | 2682 | 10,438 |
| Step 4 | 736 | 1807 | 1241 | 2139 | 1694 | 3196 | 1417 | 2544 | 10,386 |
| Step 5 | 965 | 1894 | 1379 | 1986 | 1604 | 2871 | 1288 | 2281 | 10,433 |

**Fig. 29.** The knee-lever with a corner crack; The evolutions of recovered stress on the patch of elements at the crack tip using different recovery methods at final stage of crack growth.**Fig. 30.** The knee-lever with a corner crack; A comparison between the crack trajectories obtained from the SPR and ANN techniques and that of the FEM with a very fine mesh.

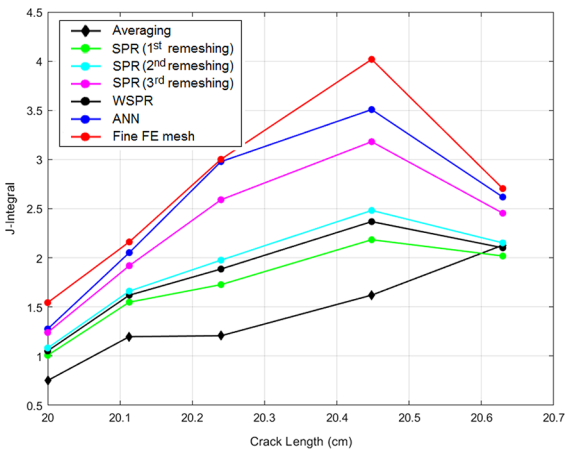


Fig. 31. The knee-lever with a corner crack; The evolutions of J -integral with the crack length using different recovery methods.

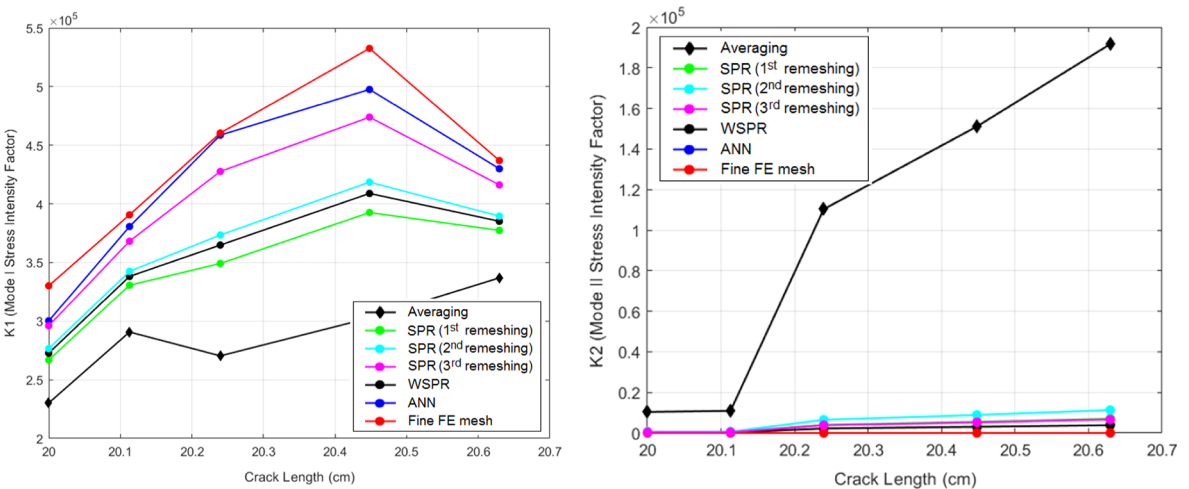


Fig. 32. The knee-lever with a corner crack; The evolutions of mode-I and mode-II stress intensity factors (K_I and K_{II}) with the crack length using different recovery methods.

Declaration of Competing Interest

None.

References

- [1] Zienkiewicz OC, Zhu JZ. A simple error estimator and adaptive procedure for practical engineering analysis. *Int J Numer Meth Eng* 1987;24:337–57.
- [2] Zienkiewicz OC, Zhu JZ. The superconvergent patch recovery and a posteriori error estimates. Part 1: the recovery technique. *Int J Numer Meth Eng* 1992;33:1331–64.
- [3] Zienkiewicz OC, Zhu JZ. Superconvergence and the superconvergent patch recovery. *Finite Elem Anal Des* 1995;19:11–23.
- [4] Wiberg NE, Abdulwahab F, Ziukas S. Enhanced superconvergent patch recovery incorporating equilibrium and boundary conditions. *Int J Numer Meth Eng* 1994;37:3417–40.
- [5] Zhang Z, Zhu JZ. Analysis of the superconvergent patch recovery technique and a posteriori error estimator in the finite element method: part II. *Comput Methods Appl Mech Eng* 1998;163:159–70.
- [6] Lee CK, Zhou CE. On error estimation and adaptive refinement for element free Galerkin method: Part I: Stress recovery and a posteriori error estimation. *Comput Struct* 2004;82:413–28.
- [7] Ródenas JJ, Tur M, Fuenmayor FJ, Vercher A. Improvement of the superconvergent patch recovery technique by the use of constraint equations: The SPR-C technique. *Int J Numer Meth Eng* 2007;70:705–27.
- [8] Khoei AR, Azadi H, Moslemi H. Modeling of crack propagation via an adaptive mesh refinement based on modified superconvergent patch recovery technique. *Eng Fract Mech* 2008;75:2921–45.
- [9] Moslemi H, Khoei AR. 3D adaptive finite element modeling of non-planar curved crack growth using the weighted superconvergent patch recovery method. *Eng Fract Mech* 2009;76:1703–28.
- [10] Payen DJ, Bathe KJ. A stress improvement procedure. *Comput Struct* 2012;112:311–26.
- [11] González-Estrada OA, Nadal E, Ródenas JJ, Kerfriden P, Bordas SA, Fuenmayor FJ. Mesh adaptivity driven by goal-oriented locally equilibrated superconvergent patch recovery. *Comput Mech* 2014;53:957–76.

- [12] Kumar S, Fourment L, Guedoux S. Parallel, second-order and consistent remeshing transfer operators for evolving meshes with superconvergence property on surface and volume. *Finite Elem Anal Des* 2015;93:70–84.
- [13] Kumar M, Kvamsdal T, Johannessen KA. Superconvergent patch recovery and a posteriori error estimation technique in adaptive isogeometric analysis. *Comput Methods Appl Mech Eng* 2017;316:1086–156.
- [14] Sharma R, Zhang J, Langelaar M, Keulen F, Aragon AM. An improved stress recovery technique for low-order 3D finite elements. *Int J Numer Meth Eng* 2018;114:88–103.
- [15] Moslemi H, Tavakkoli A. A Statistical approach for error estimation in adaptive finite element method. *Int J Comput Methods Eng Sci Mech* 2018;19:440–50.
- [16] Kaveh A, Seddighian MR. A new nodal stress recovery technique in finite element method using colliding bodies optimization algorithm. *Period Polytech Civil Eng* 2019;63:1159–70.
- [17] Lins R, Proençá SP, Duarte CA. Efficient and accurate stress recovery procedure and a posteriori error estimator for the stable generalized/extended finite element method. *Int J Numer Meth Engng* 2019;119:1279–306.
- [18] Jansari C, Kannan K, Annabattula RK, Natarajan S. Adaptive phase field method for quasi-static brittle fracture using a recovery based error indicator and quadtree decomposition. *Engng Fract Mech* 2019;220:106599.
- [19] Takeuchi J, Kosugi Y. Neural network representation of finite element method. *Neural Networks* 1994;7:389–95.
- [20] Kowata N, Ćiškoski V, Kaneda K. Direct solution method for finite element analysis using Hopfield neural network. *IEEE Trans Magn* 1995;31:1964–7.
- [21] Hurtado JE. Analysis of one-dimensional stochastic finite elements using neural networks. *Probab Engng Mech* 2002;17:35–44.
- [22] Lefik M, Schrefler BA. Artificial neural network as an incremental nonlinear constitutive model for a finite element code. *Comput Methods Appl Mech Engng* 2003;192:3265–83.
- [23] Hashash YMA, Jung S, Ghaboussi J. Numerical implementation of a neural network based material model in finite element analysis. *Int J Numer Meth Engng* 2004;59:989–1005.
- [24] Hamblí R, Chamekh A, Salah HBH. Real-time deformation of structure using finite element and neural networks in virtual reality applications. *Finite Elem Anal Des* 2006;42:985–91.
- [25] Ivirma L, Vergara M, Provenzano S, Rivas F, Perez A, Fuenmayor F. Artificial neural networks application for stress smoothing in hexahedrons. *WSEAS Trans Inform Sci Appl* 2009;6:872–83.
- [26] Park YS, Kim S, Kim N, Lee JJ. Finite element model updating considering boundary conditions using neural networks. *Engng Struct* 2017;150:511–9.
- [27] Stoffel M, Bamer F, Markert B. Artificial neural networks and intelligent finite elements in nonlinear structural mechanics. *Thin-Wall Struct* 2018;131:102–6.
- [28] Ahn B, Kim J, Choi B. Artificial intelligence-based machine learning considering flow and temperature of the pipeline for leak early detection using acoustic emission. *Engng Fract Mech* 2019;210:381–92.
- [29] Li FZ, Shih CF, Needleman A. A comparison of methods for calculating energy release rates. *Engng Fract Mech* 1985;21:405–21.
- [30] Banks-Sills L, Sherman D. On the computation of stress intensity factors for three dimensional geometries by means of the stiffness derivative and J-integral methods. *Int J Fract* 1992;53:1–20.
- [31] Khoei AR. Extended Finite Element Method. Theory and Applications: John Wiley; 2015.
- [32] Ishikawa H. A finite element analysis of stress intensity factors for combined tensile and shear loading by only a virtual crack extension. *Int J Fract* 1980;16:243–6.
- [33] Bui HD. Associated path independent J-integral for separating mixed modes. *J Mech Phys Solids* 1983;31:439–48.
- [34] Erdogan F, Sih GC. On the extension of plates under plane loading and transverse shear. *J Basic Engng* 1963;4:519–1427.
- [35] Anderson TL. Fracture Mechanics, Fundamentals and Applications. Taylor & Francis; 2017.
- [36] Azadi H, Khoei AR. Numerical simulation of multiple crack growth in brittle materials with adaptive remeshing. *Int J Numer Meth Engng* 2011;85:1017–48.
- [37] Khoei AR, Eghbalian M, Moslemi H, Azadi H. Crack growth modelling via 3D automatic adaptive mesh refinement based on modified-SPR technique. *Appl Math Model* 2013;37:357–83.
- [38] Khoei AR, Yasbolaghi R, Biabanaki SOR. A polygonal finite element method for modeling crack propagation without remeshing. *Int J Fract* 2015;194:123–48.
- [39] Nelder JA, Mead R. A simplex method for function minimization. *Comput J* 1965;7:308–13.
- [40] Sharma A, Kumar SA, Kushvaha V. Effect of aspect ratio on dynamic fracture toughness of particulate polymer composite using artificial neural network. *Engng Fract Mech* 2020;228:106907.
- [41] Piotrowski AP, Osuch M, Napiorkowski MJ, Rowinski PM, Napiorkowski JJ. comparing large number of metaheuristics for artificial neural networks training to predict water temperature in a natural river. *Comput Geosci* 2014;64:136–51.
- [42] Haykin S. Neural networks, a comprehensive foundation. *Knowl Eng Rev* 1999;13:409–12.
- [43] Nguyen D, Widrow B. Improving the learning speed of 2-layer neural networks by choosing initial values of the adaptive weights. *Proc Int Joint Conf Neural Networks* 1990;3:21–6.
- [44] Shiralinezhad V, Moslemi H. An optimized mesh partitioning in FEM based on element search technique. *Comput Concr* 2019;23:311–20.